Available online at www.sciencedirect.com
ScienceDirect
Journal of Sound and Vibration 321 (2009) 786–812
JOURNAL OF SOUND AND VIBRATION
www.elsevier.com/locate/jsvi

Experimental validation of a numerical model for subway induced vibrations

S. Gupta*, G. Degrande, G. Lombaert

Department of Civil Engineering, K.U. Leuven, Kasteelpark Arenberg 40, B-3001 Leuven, Belgium

Received 2 February 2008; received in revised form 8 August 2008; accepted 15 October 2008
Handling Editor: C.L. Morfey
Available online 30 November 2008

Abstract

This paper presents the experimental validation of a coupled periodic finite element–boundary element model for the prediction of subway induced vibrations. The model fully accounts for the dynamic interaction between the train, the track, the tunnel and the soil. The periodicity or invariance of the tunnel and the soil in the longitudinal direction is exploited using the Floquet transformation, which allows for an efficient formulation in the frequency–wavenumber domain. A general analytical formulation is used to compute the response of three-dimensional invariant or periodic media that are excited by moving loads.

The numerical model is validated by means of several experiments that have been performed at a site in Regent's Park on the Bakerloo line of London Underground. Vibration measurements have been performed on the axle boxes of the train, on the rail, the tunnel invert and the tunnel wall, and in the free field, both at the surface and at a depth of 15 m. Prior to these vibration measurements, the dynamic soil characteristics and the track characteristics have been determined. The Bakerloo line tunnel of London Underground has been modelled using the coupled periodic finite element–boundary element approach and free field vibrations due to the passage of a train at different speeds have been predicted and compared to the measurements.

The correspondence between the predicted and measured response in the tunnel is reasonably good, although some differences are observed in the free field. The discrepancies are explained on the basis of various uncertainties involved in the problem. The variation in the response with train speed is similar for the measurements as well as the predictions.

This study demonstrates the applicability of the coupled periodic finite element–boundary element model to make realistic predictions of the vibrations from underground railways.

1. Introduction

Subway induced vibrations are a matter of growing concern in densely populated cities. The interaction between the wheels and the rails induces dynamic loads on the track, which generate waves that propagate through the tunnel and the surrounding soil into buildings. Residents in buildings may perceive these

*Corresponding author.
E-mail address: shashank.gupta@bwk.kuleuven.be (S. Gupta).

0022-460X/$ - see front matter © 2008 Elsevier Ltd. All rights reserved.
doi:10.1016/j.jsv.2008.10.014

vibrations directly or indirectly in the form of re-radiated noise. Vibrations may also interfere with sensitive equipment used in research laboratories or hospitals. The frequency range of interest for subway induced vibrations is 1–80 Hz, while that of re-radiated noise is 16–250 Hz.

Great efforts have been made in the last two decades to develop models for prediction of ground-borne vibrations. Recently, Yang et al. [1] have reviewed studies on ground-borne vibrations with emphasis on those induced by underground railways. Empirical methods and simplified deterministic models are extensively used to quantify these vibrations. Empirical laws are usually derived from a vast data set collected from elaborate measurement campaigns on a number of sites [2–4]. Trochides [5] has proposed a method based on approximate impedance formulae for the tunnel–soil–building system and on energy considerations. He has compared the predictions to measurements on a scaled model.

Deterministic models comprise two-dimensional [6–9] and three-dimensional models [10–12] based on the finite element method, the boundary element method or the coupled finite element–boundary element method [13,14]. Two-dimensional models necessitate important simplification to translate the three-dimensional (moving) load into an equivalent two-dimensional load and also underestimate geometric damping in the soil. Furthermore, the wave transmission in the direction of the tunnel axis is not accounted for in two-dimensional models. The main disadvantage of three-dimensional models is that they become prohibitively large for application in the wide frequency range under consideration.

To overcome the shortcomings of two-dimensional and three-dimensional models, two-and-a-half-dimensional and periodic models are often preferred. These models solve the three-dimensional dynamic track–tunnel–soil interaction in an efficient way, assuming that the geometry in the longitudinal direction is invariant or periodic. Most of these advanced models account for three-dimensional dynamic track–tunnel–soil interaction. A two-and-a-half-dimensional model based on the coupled finite element–boundary element approach has been developed by Sheng et al. [15] and Andersen et al. [16]. The model uses the Fourier transform to formulate the problem in the frequency–wavenumber domain and is based on a subdomain formulation where the finite element method is used for the track and tunnel, while the boundary element method is used for the soil. Some researchers have also used a two-and-a-half-dimensional finite/infinite element approach to model ground-borne vibrations [17,18]. The response to moving loads in case of invariant domains has been derived by Lombaert et al. [19,20].

Within the framework of the CONVURT project [21], two numerical models have been developed: the pipe-in-pipe model [22–24] and the coupled periodic finite element–boundary element model [25,26]. The pipe-in-pipe model is a two-and-a-half-dimensional model that assumes the geometry in the longitudinal direction to be invariant. The model is based on an analytical solution of the shell equations for the tunnel and the wave equations for an elastic continuum representing the soil. The coupled periodic finite element–boundary element model uses the Floquet transform to exploit the periodicity (or invariance) in the longitudinal direction. Even though periodicity of the track–tunnel–soil system is exploited, the coupled periodic finite element–boundary element model is still quite demanding from a computational point of view. Recently, the coupled periodic finite element–boundary element model and the pipe-in-pipe model have been compared [23,27] to validate the two different approaches of tackling the dynamic track–tunnel–soil interaction problem. The response of periodic domains subjected to moving loads has been derived by Chebli et al. [28] and applied by Gupta et al. [29] to predict the vibrations on the Beijing metro network.

This paper concentrates on the experimental validation of the coupled periodic finite element–boundary element model. Within the frame of the CONVURT project elaborate in situ vibration measurements have been performed at a site in Regent's Park situated above the north- and south-bound Bakerloo line tunnels of London Underground. Vibration measurements have been performed during engineering hours at night for 35 passages of a test train in the north-bound Bakerloo line tunnel at a speed between 20 and 50 km/h. In addition, rail and wheel roughness have been measured, while the track characteristics have been determined by rail receptance measurements [30]. The dynamic soil characteristics have been determined by in situ tests (seismic cone penetration tests (SCPT), SASW) and by laboratory testing on undisturbed samples [31]. The results of the vibration measurements have been presented by Degrande et al. [32].

The modelling of the tunnel on the Bakerloo line using the coupled periodic finite element–boundary element model has also been presented by Degrande et al. [26], where the main focus was on solving the dynamic tunnel–soil interaction problem and on explaining the transfer functions. In the present paper,

this tunnel–soil model is improved for the purpose of experimental validation and the track is incorporated in the tunnel. The response of the track–tunnel–soil system during the passage of a test train in the Bakerloo line tunnel at different speeds is computed and compared to the measurements.

Lombaert et al. [20] have experimentally validated a model for railway induced vibrations by means of tests performed on the HST track on the line L2 between Brussels and Köln. They have highlighted the importance of the dynamic train–track interaction to determine the excitation forces. Sheng et al. [33] have considered experiments at three different sites: Ledsgard in Sweden (soft soil), Via Tedelda in Italy and Burton Joyce in Nottinghamshire, United Kingdom, and have discussed the relative importance of the quasi-static and dynamic forces. In the present paper, the quasi-static as well as dynamic forces due to the wheel and rail unevenness, rail joints and the parametric excitation are considered.

As a large number of parameters related to the dynamic behavior of the vehicle, the track unevenness, the geometry and material properties of the track and the tunnel, and the dynamic soil properties are involved, there are several potential sources of uncertainty. Hunt and Hussein [34] have outlined various sources of uncertainty in the process of using numerical models for the prediction of vibration from railways and questioned the prospect of achieving a prediction accuracy of better than 10 dB. The impact of uncertainties in the soil characteristics on the prediction of ground vibrations has been studied by Schevenels et al. [35]. A difference of more than 10 dB on the transfer functions has been observed due to a 10% variation in the dynamic soil characteristics.

The objective of the present paper is two-fold. The first aim is to describe how the relevant information from the tests is extracted to model the Bakerloo line tunnel using the coupled periodic finite element–boundary element approach. The properties of the tunnel and the soil have been taken from Degrande et al. [32], while the excitation force and the track parameters are obtained by further analysis of the measurement data. Subsequently, the response to moving trains for different train speeds is computed and compared to the experimental results.

The second aim of the paper is to prosper a better understanding in the generation and propagation mechanism of vibrations from underground railways. Some of the important parameters, which are crucial for the accurate prediction of the ground-borne vibrations are highlighted. The discrepancies in the predictions and the measurements are explained.

The paper is organized in the following manner. Section 2 briefly describes the methodology for predicting ground-borne vibrations from underground railways. The modelling of the Bakerloo line tunnel using the coupled finite element–boundary element model is described and the computation of the transfer functions and the wheel/rail interaction forces is discussed. Emphasis has been given on the determination of the dynamic forces from the measured roughness and the axle box vibrations. Section 3 presents the results for the simulations, where the response in the tunnel and the free field is predicted and validated for the passage of a train at a speed of 47.6 km/h. The validation of the response for other train speeds and the study of variation of the response with train speed are presented in Section 4.

2. The numerical method

Within the frame of the CONVURT project [21], a coupled periodic finite element–boundary element model has been developed that exploits the longitudinal invariance or periodicity of the track–tunnel–soil system [25,26]. The three-dimensional dynamic tunnel–soil interaction problem is solved with a subdomain formulation, using a finite element method for the tunnel and a boundary element method for the soil, modelled as a horizontally layered elastic halfspace. The response to moving loads is deduced from the frequency content of the axle loads and the transfer functions in the frequency–wavenumber domain [20,28,29].

2.1. Response due to moving loads

In the fixed frame of reference, the distribution of n_a vertical axle loads moving in the longitudinal direction $\mathbf{e}_y$ on the coupled track–tunnel–soil system is written as the summation of the product of Dirac functions that determine the time-dependent position $\mathbf{x}_k = \{x_{k0}, y_{k0} + vt, z_{k0}\}^{\mathrm{T}}$ and the time history $g_k(t)$ of the

k-th axle load:

$$\rho\mathbf{b}(\mathbf{x},t)=\sum_{k=1}^{n_a}\delta(x-x_{k0})\delta(y-y_{k0}-vt)\delta(z-z_{k0})g_k(t)\mathbf{e}_z \tag{1}$$

y_{k0} is the initial position of the k-th axle that moves with the train speed v along the y-axis and $\mathbf{e}_z$ denotes the vertical unit vector.

An infinite periodic structure can be analyzed using the Floquet transform [25,26] by restricting the problem domain Ω to a single periodic unit or reference cell $\tilde{\Omega}$. If the spatial period is L, then the position $\mathbf{x}$ of any point in the problem domain is decomposed as $\mathbf{x}=\tilde{\mathbf{x}}+nL\mathbf{e}_y$, where $\tilde{\mathbf{x}}$ is the position in the reference cell and n is the cell number. The response to moving loads in case of periodic domains is given by [28,29,36]

$$\hat{u}_i(\tilde{\mathbf{x}}+nL\mathbf{e}_y,\omega)=\frac{1}{2\pi}\sum_{k=1}^{n_a}\int_{-\infty}^{\infty}\hat{g}_k(\omega-k_yv)\exp[-\mathrm{i}k_y(nL-y_{k0})]\int_{-L/2}^{L/2}\exp(-\mathrm{i}k_y\tilde{y}')\tilde{\hat{h}}_{zi}(\tilde{\mathbf{x}}',\tilde{\mathbf{x}},\kappa_y,\omega)\,\mathrm{d}\tilde{y}'\,\mathrm{d}k_y \tag{2}$$

where $\kappa_y=k_y-2m\pi/L$. The transfer function $\tilde{\hat{h}}_{zi}(\tilde{\mathbf{x}}',\tilde{\mathbf{x}},\kappa_y,\omega)$ in the frequency–wavenumber domain is the Floquet transform of the transfer function $\hat{h}_{zi}(\tilde{\mathbf{x}}',\tilde{\mathbf{x}}+nL\mathbf{e}_y,\omega)$ in the frequency–spatial domain [25,26]. It can be seen from Eq. (2) that the transfer function $\tilde{\hat{h}}_{zi}(\tilde{\mathbf{x}}',\tilde{\mathbf{x}},\kappa_y,\omega)$ and the frequency content of the axle load $\hat{g}_k(\omega)$ are needed to compute the response to moving loads.

The transfer functions are computed by means of the coupled periodic finite element–boundary element model using the classical domain decomposition approach based on the finite element method for the tunnel and the boundary element method for the soil [26], while the axle loads are computed by solving a wheel–track interaction problem.

2.2. Characteristics of the vehicle, track, tunnel and soil

The Bakerloo line tunnel of London Underground is a deep bored tunnel with a cast iron lining and a single track, embedded in London clay at a depth of 28 m. The tunnel has an internal radius of 1.83 m and a wall thickness of 0.022 m (Fig. 1). There are six longitudinal stiffeners and one circumferential stiffener at an

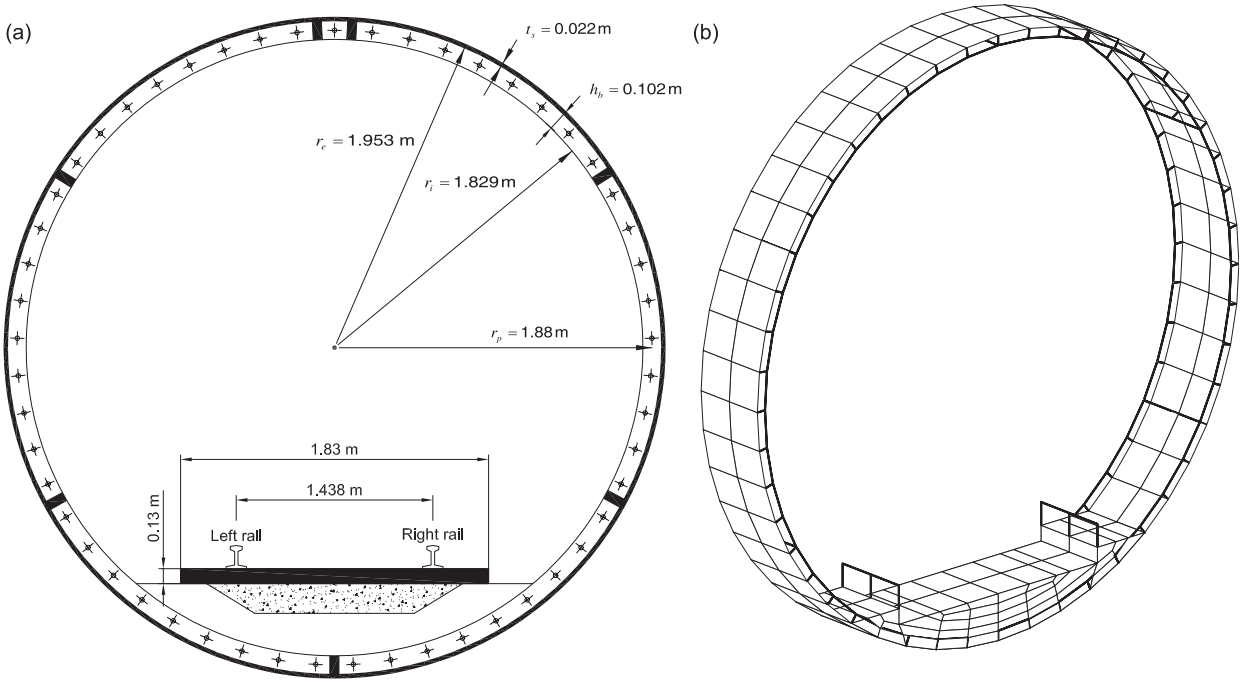

Fig. 1. (a) Cross section of the metro tunnel on the Bakerloo line at Regent's Park. (b) Finite element model of the reference cell.

interval of 0.508 m, resulting in a periodic structure. The Floquet transform is used to exploit the periodicity of the geometry and to restrict the problem domain to a single bounded reference cell [26]. The finite element model of the reference cell is made using the general purpose finite element program ANSYS. Fig. 1b shows the finite element model of the tunnel's reference cell, where shell elements have been used for the cast iron lining, while the longitudinal and circumferential stiffeners are modelled using beam elements. The concrete on the tunnel invert has been modelled using 8-node brick elements with incompatible bending modes. The size of the finite elements is governed by the boundary element mesh along the tunnel–soil interface, so that ideally a minimum of $N = 8$ elements are used per minimum shear wavelength $\lambda_s^{\min} = C_s/f_{\max}$, with $C_s = 325\,\mathrm{m/s}$ the shear wave velocity in the soil layer around the apex of the tunnel and $f_{\max} = 100\,\mathrm{Hz}$ the maximum excitation frequency of interest. This results in a recommended element length $l_e = \lambda_s^{\min}/N = 0.40\,\mathrm{m}$. In the present model, two elements are used in the longitudinal direction ($l_e = 0.2540\,\mathrm{m}$), while 48 elements are used to model the tunnel lining in the circumferential direction ($l_e = 0.2395\,\mathrm{m}$).

The soil is modelled as an elastodynamic medium, which is characterized by the shear modulus, Poisson's ratio, the density and the material damping ratio. Various damping models can be used for the analysis. In structural mechanics, viscous damping models are frequently used. Viscous damping is rate dependent and the energy dissipation increases with the frequency. In soil dynamics, material damping is usually assumed to be rate independent in the low frequency range and a hysteretic material damping model is widely used for applications in the frequency domain, using complex Lamé coefficients [37].

Dynamic soil characteristics have been determined by in situ tests (SASW, SCPT, CPT) as well as by laboratory tests on undisturbed samples (bender element test, free torsion pendulum test) [31,32]. The seismic cone penetration tests (SCPT) were performed at four locations in the free field FF02, FF04, FF07 and FF09 (Fig. 10). The classical cone penetration tests were also performed at the same points, to measure the cone resistance and friction ratio. These tests have revealed that the tunnel is embedded in a layered soil consisting of a single shallow layer with a thickness of 5 m on top of a homogeneous halfspace consisting of London clay. The top layer is not very homogeneous, and soil characteristics differ considerably at different measurement points in the free field. For the computations, the top layer is assumed homogeneous, with a shear wave velocity $C_s = 325\,\mathrm{m/s}$, a longitudinal wave velocity $C_p = 1964\,\mathrm{m/s}$, a density $\rho_s = 1980\,\mathrm{kg/m^3}$ and a material damping ratio $\beta_s = 0.042$. The underlying halfspace has a shear wave velocity $C_s = 220\,\mathrm{m/s}$, a longitudinal wave velocity $C_p = 1571\,\mathrm{m/s}$, a density $\rho_s = 1980\,\mathrm{kg/m^3}$ and a material damping ratio $\beta_s = 0.039$. The material damping ratio is determined by means of free torsion pendulum tests in the laboratory. The accurate determination of the material damping ratio is important for reliable predictions of ground vibrations [38]. However, the uncertainty associated with the material damping ratio is high and the predictions in the free field are expected to be less reliable. Moreover, as the tunnel is situated at a considerable depth, the dynamic soil properties around the tunnel could not be precisely estimated. It has been assumed that the tunnel is embedded in a homogeneous layer of London clay. The soil in the immediate vicinity of the tunnel strongly influences the wave propagation from the tunnel in all directions, thus, uncertainty remains in the prediction of the free field vibrations.

The track is a non-ballasted concrete slab track with Bullhead rail supported on hard wooden sleepers nominally spaced at $d = 0.95\,\mathrm{m}$ with cast iron chairs. Both ends of a sleeper are concreted into the invert and the space between the sleepers is filled with shingle. The shingle does not support the sleepers but only provides drainage and facilitates evacuation in case of an emergency. The shingle can be modelled as an added mass on the tunnel invert, but has been ignored as its mass is substantially less than the mass of the tunnel and the concrete invert. The rails have a mass per unit length $\rho_r A_r = 47\,\mathrm{kg/m}$ and a bending stiffness $E_r I_r = 3.04 \times 10^6\,\mathrm{N\,m^2}$. The rails are not supported by rail pads and the resilience is mainly provided by the bending of the timber sleepers, which have a varying stiffness depending on their moisture content. An invariant track model instead of a periodic one is used in the present analysis, where the mass and stiffness properties of the discretely supported track are uniformly distributed in the longitudinal direction. A comparison between homogeneous and periodic track models has been made by several researchers [39–41]. The conclusion of these studies has been that the continuously supported models are appropriate for the vertical track dynamics in the low frequency range between 1 and 100 Hz. In the present case, the dynamic behavior of the track has also been studied using a homogeneous track model as the pinned–pinned resonance occurs at a frequency well above 100 Hz. The track model consists of two infinite Euler beams representing the

two rails and mass elements representing the sleepers. The mass of the sleepers is distributed in the longitudinal direction with a mass per unit length $m_s = M_s/d = 70\,\mathrm{kg/m}$. As there are no rail pads, a stiff connection is assumed between the rails and the sleepers, while the sleepers are continuously supported on the tunnel invert with springs, whose stiffness and damping values are determined from rail receptance measurements. The continuous elastic support below the sleepers accounts for the resilience in the track. If the stiffness of the track is much lower than the stiffness of the track bed, the track bed can be considered as a rigid foundation for calculating the rail receptance. Thus, the model of a track on a rigid base is used to calculate the rail receptance in the frequency range between 1 and 500 Hz. Fig. 2 shows the measured and the computed receptance of the rail. The stiffness $\bar{k}_s = k_s/d = 100\,\mathrm{MN/m^2}$ and damping $\bar{c}_s = 15 \times 10^4\,\mathrm{N\,s/m^2}$ in the elastic support are used to calculate the rail receptance. The computed receptance is close to the measured receptance at frequencies above 200 Hz. The receptance measured at mid span between the sleepers shows a pinned–pinned resonance frequency of 380 Hz, which is not visible in the calculated results, as a homogeneous model of the track has been assumed. At frequencies below 150 Hz, the measured rail receptance is not reliable as the coherence of the measurements is low. A high value of the damping is used to suppress the resonance, as no resonance has been observed in the rail receptance measurements within 300 Hz. The choice of the track parameters will be further justified by observing the wheel–track resonance frequency and the quasi-static response on the rail.

The test train employed for vibration measurements on the Bakerloo line consists of seven cars: a driving motor car, a trailer car, two non-driving motor cars, two trailer cars and a driving motor car. Fig. 3 shows the composition of the first three cars of the test train. The length of a motor car is $L_t = 16.09\,\mathrm{m}$, while the length of the trailer car is $L_t = 15.98\,\mathrm{m}$. The bogie distance L_b on all cars is 10.34 m, while the axle distance $L_a = 1.91\,\mathrm{m}$. The distance between the first and the last axle of the train is 108.33 m. The wheels are of the monobloc type and have a diameter of about 0.70 m. The tare mass of a motor car is 15330 kg, while the bogie mass is 6690 kg and the mass of wheelset is 1210 kg. The tare mass of a trailer car is 10600 kg, while the bogie mass is 4170 kg and the mass of a wheelset is 950 kg. The carriage length L_t, the distance L_b between bogies, the axle distance L_a, the total axle mass M_t, the sprung axle mass M_s and the unsprung axle mass M_u of the motor car and the trailer car are summarized in Table 1.

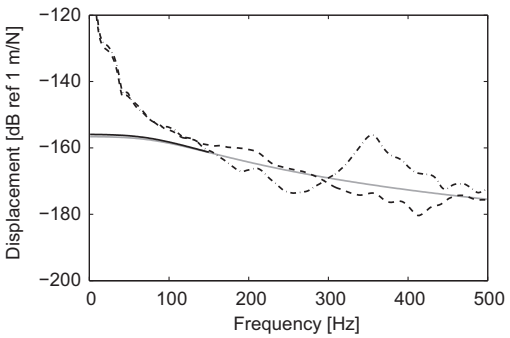

Fig. 2. The rail receptance measured over the sleeper (dashed line) and at mid span between the sleepers (dash-dotted line) and the rail receptance computed from the model of the track on a rigid base (gray line) and from the full three-dimensional track–tunnel–soil model (solid black line).

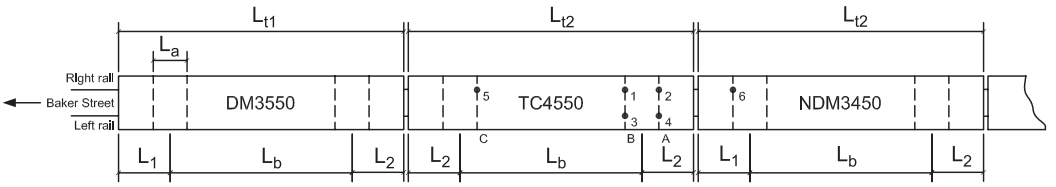

Fig. 3. Composition of the first three cars of the test train and position of the wheelsets A, B and C on the trailer car, as well as the numbering of the axle boxes.

Table 1
Geometrical and mass characteristics of the test train.

	L_t (m)	L_b (m)	L_a (m)	M_t (kg)	M_s (kg)	M_u (kg)
Motor car	16.09	10.34	1.91	8387.5	7177.5	1210
Trailer car	15.98	10.34	1.91	5685	4735	950

2.3. Transfer functions

As the reference cell of the tunnel is bounded, the tunnel displacements $\tilde{\mathbf{u}}_t(\tilde{\mathbf{x}}, \kappa_y, \omega)$ are decomposed on a basis of functions $\tilde{\boldsymbol{\Psi}}_t(\tilde{\mathbf{x}}, \kappa_y)$, while the soil displacements $\tilde{\mathbf{u}}_s(\tilde{\mathbf{x}}, \kappa_y, \omega)$ are written as the superposition of waves that are radiated by the tunnel into the soil.

The weak or variational formulation of the problem results in the following system of equations in the frequency–wavenumber domain [25,26,42]:

$$[\mathbf{K}_t(\kappa_y) - \omega^2 \mathbf{M}_t(\kappa_y) + \mathbf{K}_s(\kappa_y, \omega)]\boldsymbol{\alpha}(\kappa_y, \omega) = \mathbf{F}_t(\kappa_y, \omega) \tag{3}$$

where $\mathbf{K}_t(\kappa_y)$ and $\mathbf{M}_t(\kappa_y)$ are the projection of the finite element stiffness matrix and mass matrix of the tunnel's reference cell on the tunnel modes $\tilde{\boldsymbol{\Psi}}_t(\tilde{\mathbf{x}}, \kappa_y)$, while $\mathbf{K}_s(\kappa_y, \omega)$ is the dynamic stiffness matrix of the soil calculated with a periodic boundary element formulation with Green–Floquet functions defined on the periodic structure with period L along the tunnel [25,42].

Eq. (3) is solved to obtain the displacement field in the reference cell in the frequency–wavenumber domain. The displacements in the frequency-spatial domain are obtained using the inverse Floquet transform [25,26].

The Craig–Bampton substructuring technique is used to efficiently incorporate a track in the tunnel [26,29]. The kinematics of the track-tunnel system are described as a superposition of track modes on a rigid base and the quasi-static transmission of free tunnel modes into the track. The advantage of this approach is that the dynamic stiffness of the soil only depends on the periodic tunnel modes and does not change when alternative track structures are considered. Gupta et al. [43] have described three strategies to select the kinematical basis $\tilde{\boldsymbol{\Psi}}_t(\tilde{\mathbf{x}}, \kappa_y)$. The strategy used in this paper involves the computation of eigenmodes of the tunnel's reference cell after imposing the periodicity condition of the second kind. This results in a complex wavenumber-dependent eigenvalue problem, which should be solved at each wavenumber. To reduce the computational effort, the complex eigenvalue problem is solved for only a few lower modes M at selected wavenumbers $[\kappa_{y1}, \kappa_{y2}, \ldots, \kappa_{yq}]$ in the range $[0, \pi/L]$. These eigenvectors are collected in a matrix and a singular value decomposition is applied to obtain the kinematical basis $\tilde{\boldsymbol{\Psi}}_t$. In the present case, 84 periodic modes of the second kind [26] are determined and used for the computation, which include 60 free tunnel modes and 24 track modes on a rigid base. The number of modes is large enough to obtain the converged solution.

Fig. 2 also shows the rail receptance in the frequency range between 1 and 150 Hz, calculated from a full three-dimensional dynamic track–tunnel–soil interaction problem. It is shown that the rail receptance computed from this approach is the same as calculated from the track model on a rigid base.

The wave field radiated into the soil is computed using the dynamic representation theorem in the unbounded soil domain corresponding to the reference cell. The transfer functions in the frequency–wavenumber domain are used in Eq. (2) to compute the incident wave field due to a moving train.

In the following, the transfer functions are calculated with a load of 0.5 N on each rail to account for the equal distribution of the train load on both rails. Fig. 4 shows the transfer function at the tunnel invert, in the free field at 5.5 and 23.3 m from the tunnel, on the surface, and at 23.3 m from the tunnel, at a depth of 15 m. The transfer functions give an insight into the wave propagation in the free field. Superimposed on these graphs are Green's functions of the layered halfspace with the same properties as the soil where the tunnel is embedded. The transfer function at the tunnel invert does not show any marked resonance due to the dynamic tunnel–soil interaction and the dissipation of energy due to material and geometrical damping in the soil. The experimental transfer functions are not available from the measurement campaign and thus, the experimental validation of the transfer functions is not possible. The transfer functions in the free field (Figs. 4b–d) are similar to that of a point load applied in a layered halfspace as the tunnel has a small diameter and is situated

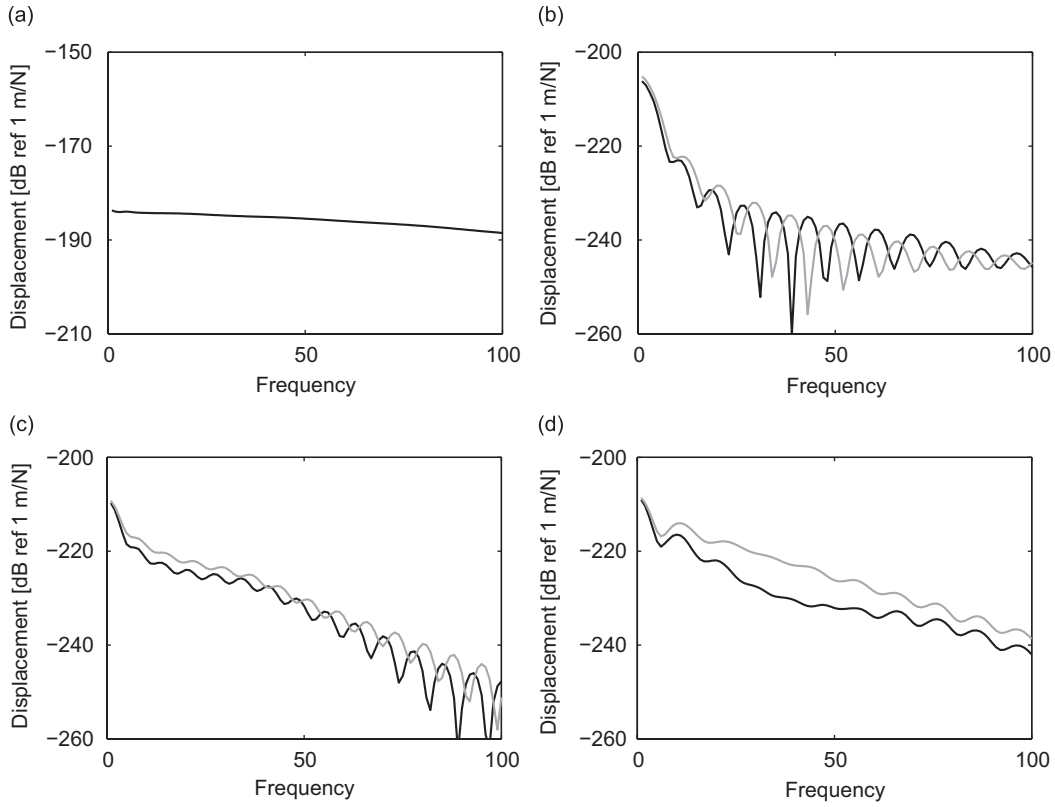

Fig. 4. (a) Vertical transfer function (a) at the tunnel invert and in the free field at (b) $\{5.5\,\mathrm{m}, 0\,\mathrm{m}, 0\,\mathrm{m}\}^{\mathrm{T}}$, (c) $\{23.3\,\mathrm{m}, 0\,\mathrm{m}, 0\,\mathrm{m}\}^{\mathrm{T}}$ and (d) $\{23.3\,\mathrm{m}, 0\,\mathrm{m}, -15\,\mathrm{m}\}^{\mathrm{T}}$. Superimposed on (b)–(d) are Green's functions of the layered halfspace (gray line).

at a considerable depth. At low frequencies, the dynamic stiffness of the soil is larger than the dynamic stiffness of the tunnel and, therefore, the response in the free field is strongly influenced by the dynamic characteristics of the soil. It can be observed that, at frequencies below 10 Hz, the transfer functions of the track–tunnel–soil system are identical to Green's function of the layered halfspace. At higher frequencies the dynamic stiffness of the tunnel becomes important and the response in the free field becomes different from Green's functions. The track resonance occurs at a frequency higher than 100 Hz and, therefore, its effect is not visible in the frequency range between 1 and 100 Hz. As the observation points are located far from the tunnel, the response is primarily due to the waves emanating from the tunnel. The transfer functions as well as Green's functions of the layered halfspace on the surface are characterized by an undulating behavior, which is due to the interference of compression and shear or Rayleigh waves. Furthermore, it can be observed that higher frequency components are decaying more rapidly with increasing distance from the tunnel, due to material damping in the soil.

The response of the system has not been affected by the periodicity of the tunnel in the frequency range between 1 and 100 Hz. The effect of the spatial periodicity such as stop bands would occur at much higher frequencies. Therefore, the tunnel can also be modelled as an equivalent invariant structure and two-and-a-half-dimensional methods can be employed for tackling this problem. However, in the present study the coupled periodic finite element–boundary element model has been used which allows to conveniently model a periodic geometry. This approach has the advantage that the existing three-dimensional boundary element technology for layered media can be reused, as the periodic Green's kernels have the same singularities as the three-dimensional Green's kernels [25,42]. The two-and-a-half-dimensional approach would have necessitated the analysis of the singularities of the two-and-a-half-dimensional Green's functions, which is now avoided by using the Green-Floquet functions.

2.4. The wheel–track interaction forces

Ground-borne vibrations from moving trains can be attributed to various excitation mechanisms. A distinction is made between the quasi-static and dynamic contribution, decomposing the time history $g_k(t) = g_{ks} + g_{kd}(t)$ of each axle load into a static component g_{ks} and a dynamic component $g_{kd}(t)$. For the experimental validation of the numerical model, four excitation mechanisms are considered to be important: the quasi-static excitation, the unevenness excitation due to wheel and rail roughness, the impact excitation due to rail joints and the parametric excitation due to sleeper periodicity.

2.4.1. Quasi-static forces

The quasi-static excitation occurs when successive axles of the train pass over the track and can be modelled as constant forces moving along the track with the train speed v. The constant load g_{ks} is equal to the axle weight w_k. The Fourier transform $\hat{g}_{ks}(\omega)$ equals $2\pi w_k \delta(\omega)$. The frequency content of the free field displacements is obtained by substituting $\hat{g}_k(\tilde{\omega})$ in Eq. (2). According to the properties of the vehicle, the resulting axle loads on the trailer car and the motor car are 55.77 and 82.28 kN, respectively.

2.4.2. Dynamic forces

The main excitation mechanisms that give rise to dynamic forces are the random excitation due to rail and wheel unevenness, the impact excitation due to rail joints and wheel flats and the parametric excitation due to sleeper periodicity.

For the simple case of the vertical interaction between the wheel and the rail, the contact forces $\hat{\mathbf{g}}_d(\omega)$ in the frequency domain are given as [20]:

$$[\hat{\mathbf{C}}^v(\omega) + \hat{\mathbf{C}}^t(\omega)]\hat{\mathbf{g}}_d(\omega) = -\hat{\mathbf{u}}_{w/r}(\omega) \tag{4}$$

where $\hat{\mathbf{u}}_{w/r}(\omega)$ is the relative displacement (unevenness) between the wheel and the rail, while $\hat{\mathbf{C}}^v(\omega)$ and $\hat{\mathbf{C}}^t(\omega)$ are the compliance of the vehicle and the track, respectively.

The frequency content of the rail and wheel unevenness $\hat{\mathbf{u}}_{w/r}(\omega)$ is calculated from the wavenumber domain representation $\tilde{u}_{w/r}(k_y)$ of the unevenness $u_{w/r}(y)$. The parametric excitation and the excitation due to rail joints and wheel flats can also be accounted for by Eq. (4), where $\hat{\mathbf{u}}_{w/r}(\omega)$ is the equivalent unevenness perceived by the moving vehicle. It should be emphasized that Eq. (4) is only valid for longitudinally invariant media and the parametric excitation can only be included indirectly through the unevenness term $\hat{\mathbf{u}}_{w/r}(\omega)$. Moreover, as the rail receptance of a discretely supported track and a continuously supported track are approximately the same at frequencies well below the pinned–pinned resonance, the homogeneous track model can be used for the predictions.

The train can be well represented with the vehicle's unsprung mass, as the vehicle's primary and secondary suspensions isolate the body and the bogie from the wheel set at frequencies above a few Hertz. In this case, the vehicle compliance matrix is equal to a diagonal matrix $\hat{\mathbf{C}}^v(\omega) = \mathrm{diag}\{-1/(M_u\omega^2)\}$ of order 28. Since the vehicle compliance is assumed to be a diagonal matrix, the coupling between the axles on the same bogie, known as leakage, is ignored, although a moderate coupling was observed in the experimental results. Also the effect of through axle coupling was observed, indicating a strong coupling between the wheels of the same axle.

The track compliance $\hat{\mathbf{C}}^t(\omega)$ is calculated in the fixed frame of reference as the maximum train speed considered is 47.6 km/h, which is much less than the critical speed of the track-tunnel-soil system. Like the transfer functions, the track compliance is computed for a load of 0.5 N on both rails. The element $\hat{C}^t_{lk}(\omega)$ of the track compliance matrix represents the track response at the position of axle l due to the applied load at axle k.

The displacements of the axles are related to the excitation forces $\hat{\mathbf{g}}_d(\omega)$ and the vehicle compliance $\hat{\mathbf{C}}^v(\omega)$ as [20]

$$\hat{\mathbf{C}}^v(\omega)\hat{\mathbf{g}}_d(\omega) = -\hat{\mathbf{u}}_a(\omega) \tag{5}$$

Fig. 5 shows the displacement $\hat{u}_a(\omega)$ of an axle of the motor car, due to the interaction between the axle and the track for a unit roughness $\hat{u}_{w/r}(\omega) = 1$. At the wheel–track resonance, which occurs at a frequency of 52 Hz, the imposed displacement is taken by the vehicle, while the track displacement tends to zero [20]. From the vibration measurements on the rail and on the axle boxes of the train, it has also been observed that the

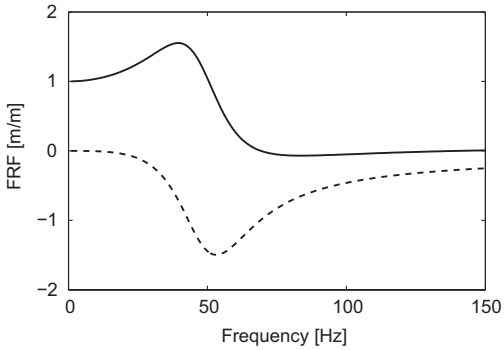

Fig. 5. Real (solid line) and imaginary (dashed line) part of an axle displacement $\hat{u}_a$ for a unit impulse excitation.

wheel–track resonance frequency is situated between 50 and 60 Hz. This further confirms the choice of the track parameters.

Rail roughness has been measured using the Müller BBM rail roughness measurement equipment (RM1200E). Measurements were taken on both rails over 50 m of the track on both sides of the reference section [32]. The data were processed to produce spatial profiles and averaged one-third octave band spectra. It is seen that rail roughness dominates at low wavenumbers, while wheel roughness dominates at high wavenumbers (Ref. [32, Figures 4 and 5]). The low wavenumbers correspond to longer wavelengths and are responsible for excitation in the frequency range of interest (1–100 Hz); higher wavenumbers are important for higher frequency excitation that may give rise to re-radiated noise in buildings in the frequency range up to 250 Hz. In the present measurements, no rail unevenness with wavelengths longer than 0.1 m could be measured, restricting the analysis to frequencies above 130 Hz for a train speed of 47.6 km/h.

Axle box vibrations provide additional information about the unevenness of the track. Axle box vibrations have been measured on six axle boxes during the whole journey of the test train on the section between Regent's Park and Baker Street stations [26]. The position of these axle boxes on the train is marked in Fig. 3. Fig. 6a shows the time history of the acceleration of axle box 1 for a period of time corresponding to the passage of a train over the distance $L_r = 108.33$ m from $y = -L_r/2$ to $y = L_r/2$ at a speed of 47.6 km/h. The axle box response is affected by the combined rail and wheel unevenness, while the peaks in the response are clearly due to the passage of the axle over joints in the rail.

One-third octave band spectra of the axle box displacements can be obtained from the axle box accelerations. The axle box displacements are approximately equal to the combined rail and wheel unevenness in the lower frequency range (below the wheel–track resonance frequency), where the vehicle compliance dominates the track compliance. Fig. 6b compares the axle box displacements and the measured unevenness. Superimposed on the same graph are the TSI+ (Technical Specifications for Interoperability) [44] and ISO 3095:2005 [45] limits. The high response of the axle boxes indicates that the rails are of very poor quality. It can be observed that, even at high frequencies (short wavelengths), the measured unevenness is approximately equal to the axle box displacement.

In this paper, the wheel/rail interaction forces $\hat{\mathbf{g}}_d(\omega)$ are directly derived from the axle box displacements $\hat{\mathbf{u}}_a(\omega)$ and the vehicle compliance $\hat{\mathbf{C}}^v(\omega)$ using Eq. (5). The advantage of using Eq. (5) to estimate the interaction force is that the various excitation mechanisms such as the unevenness excitation, parametric excitation and excitation due to rail joints and wheel flats are implicitly accounted for. Moreover, Eq. (5) does not require any approximation or assumption about the unevenness in the frequency range between 1 and 80 Hz, where direct unevenness measurements are not available.

Fig. 7 shows the frequency content and the one-third octave band RMS spectrum of the wheel–rail interaction force as a function of the frequency for a train speed of 47.6 km/h. Fig. 7b also displays the one-third octave band RMS spectrum of the contact force computed using Eq. (4), where the unevenness has been approximated with axle box displacements. An overestimation of the dynamic forces around the wheel–track resonance frequency can be observed.

The frequency content of the estimated forces exhibits a clear maximum near the train-track resonance frequency between 50 and 60 Hz. The force has been estimated by considering the axle box vibrations for a

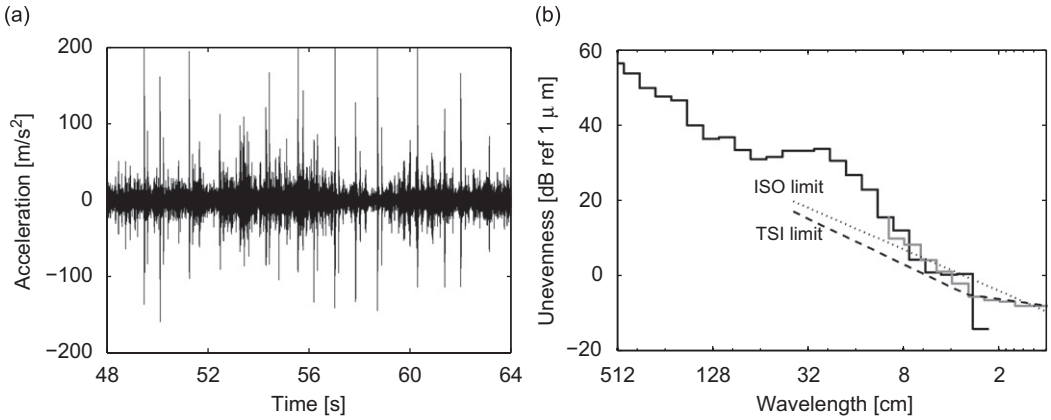

Fig. 6. (a) Time history of the vertical acceleration on axle box 1 for a period of time corresponding to the passage of a train over a distance $L_r = 108.33$ m. (b) One-third octave band unevenness spectra from the axle box vibrations (black line) and from the roughness measurements on the rails and the wheels (gray line). Superimposed on the graph are the TSI+ (dashed line) and ISO limit (dash-dotted line).

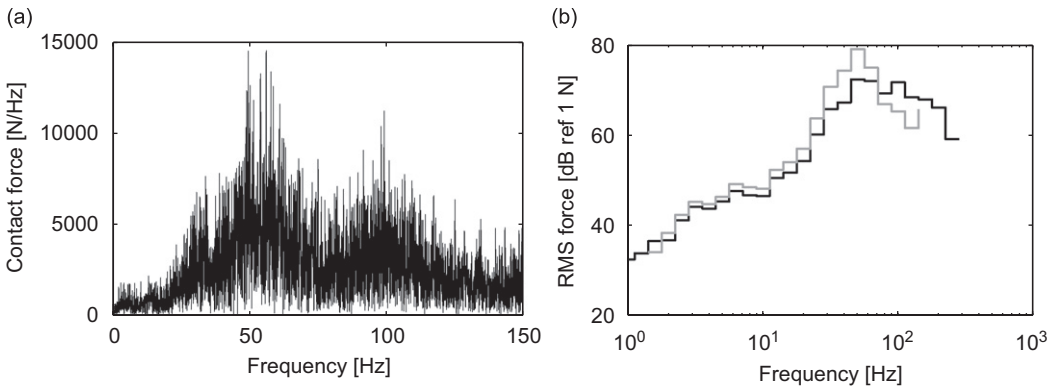

Fig. 7. (a) Frequency content and (b) one-third octave band RMS spectrum of the contact force at the front axle of the train for a speed of 47.6 km/h. Superimposed on (b) is the one-third octave band RMS spectrum of the contact force computed according to Eq. (4) (gray line).

period corresponding to the passage of the train over the distance $L_r = 108.33$ m from $y = -L_r/2$ to $y = L_r/2$. This stretch of length L_r is chosen to be symmetric about the reference section. The movement of the axle boxes along the stretch of length $2L_r = 216$ m is identified with an electronic light beam positioned on one of the axle boxes and a reflector located on a tunnel wall near the reference section [32]. It has been assumed that the response at the reference section is not significantly influenced by unevenness and joints outside this zone. It should be mentioned that the estimation of the forces is not accurate at very low frequencies below 3–4 Hz, as a band pass filter with a high-pass frequency of 3 Hz has been used in the processing of the recorded data. Moreover, the assumed vehicle model only accounts for the unsprung axle masses and is not accurate at frequencies below 10 Hz, where the train suspensions have a strong influence. The contact force has been estimated for four axles on the trailer car and one axle on the motor car, for which axle box vibrations have been measured. The contact force at other axles of a similar car are considered identical except for a phase shift. Furthermore, identical input on both rails is assumed in the analysis.

3. Response during the passage of a train in the Bakerloo line tunnel

The experiments on the Bakerloo line have been performed during 35 passages of a test train at a speed between 20 and 50 km/h. In the present section, the response to a train moving at a speed of 47.6 km/h is predicted and compared to the experimental results.

The response is calculated by adding the contribution of the dynamic forces and the quasi-static forces in the frequency domain. In the following, the time history, the frequency content, the running RMS and the one-third octave band RMS spectra of the measured and predicted vertical vibration velocity are compared.

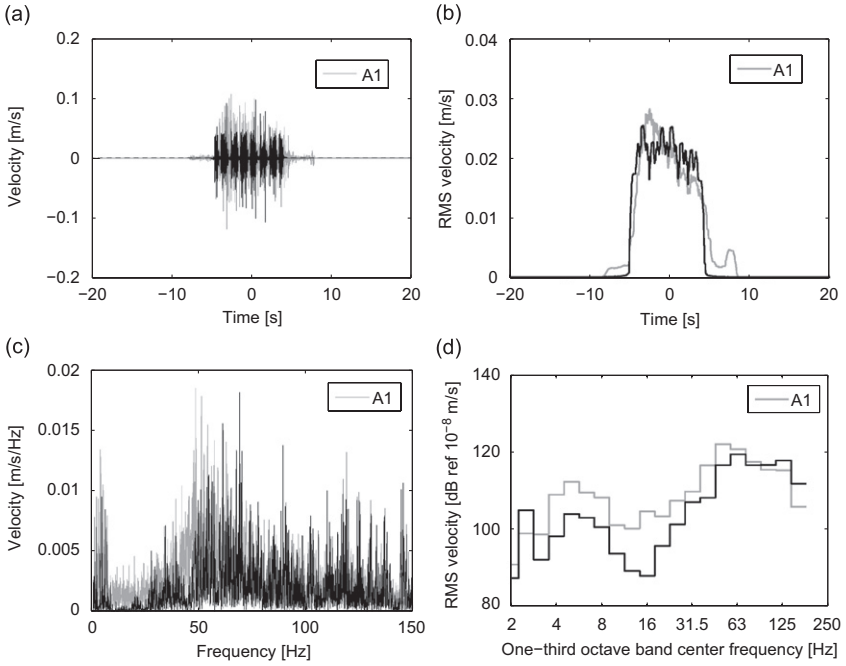

Fig. 8. Experimental (gray line) and computed (black line) (a) time history, (b) running RMS, (c) frequency content and (d) one-third octave band RMS spectra of the vertical velocity on the rail (A1) during the passage of a test train at a speed of 47.6 km/h.

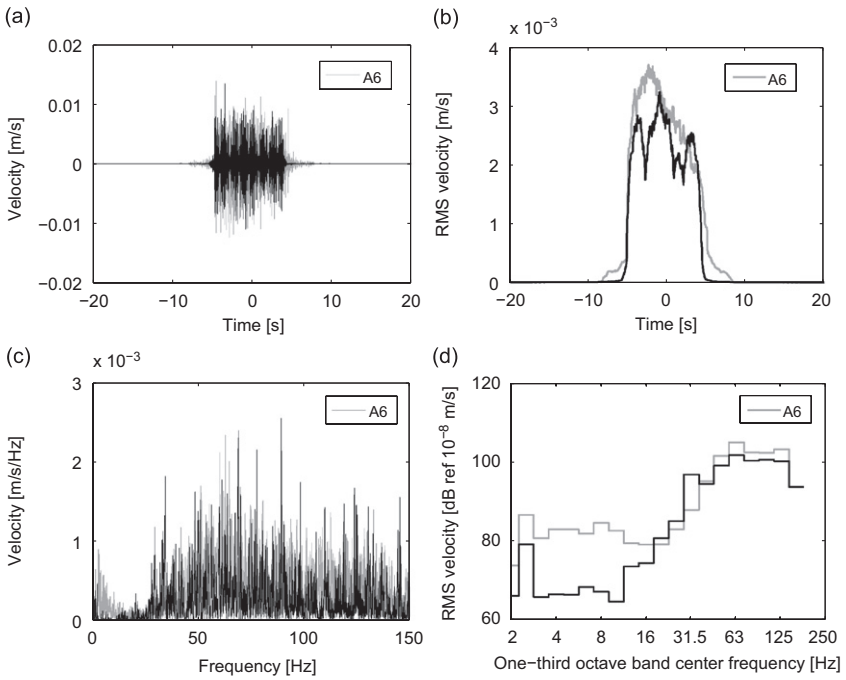

Fig. 9. Experimental (gray line) and computed (black line) (a) time history, (b) running RMS, (c) frequency content and (d) one-third octave band RMS spectra of the vertical velocity at the tunnel invert (A6) during the passage of a test train at a speed of 47.6 km/h.

The running RMS has been calculated with an averaging time of 1 s according to ISO 2631-2 [46]. The one-third octave band RMS spectra of the vertical velocity are computed according to the German standard DIN 45672-2 [47] on a reference period T_2, during which the response is considered to be stationary.

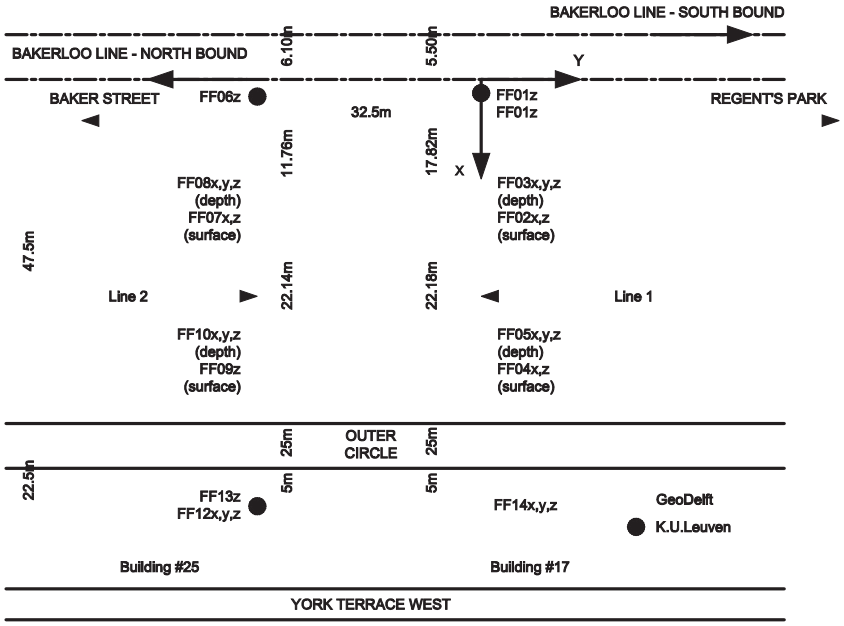

Fig. 10. Measurement setup in Regent's Park above the Bakerloo line tunnels.

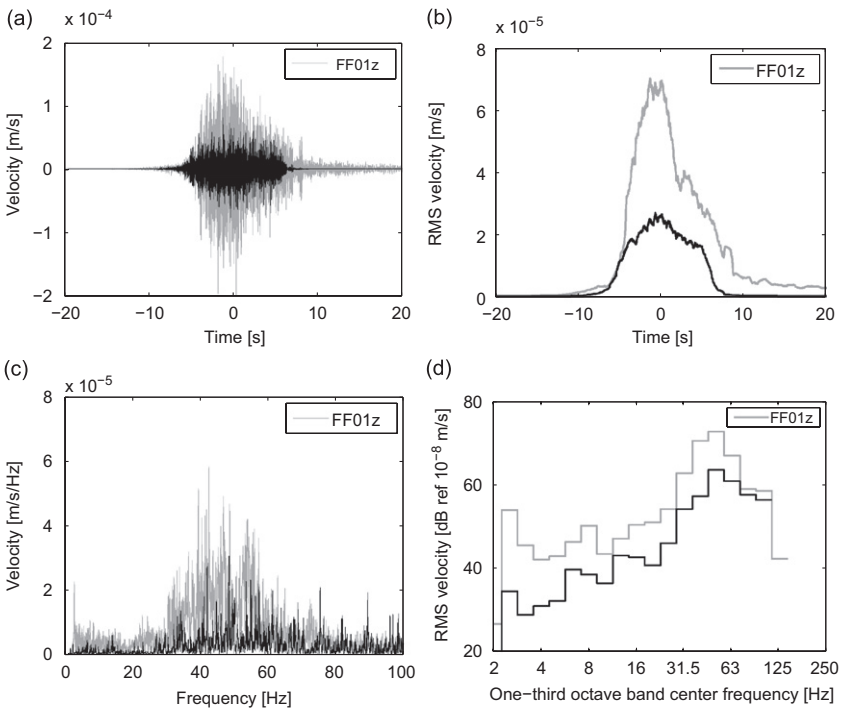

Fig. 11. Experimental (gray line) and computed (black line) (a) time history, (b) running RMS, (c) frequency content and (d) one-third octave band RMS spectra of the vertical velocity at $\{5.5\,\mathrm{m}, 0\,\mathrm{m}, 0\,\mathrm{m}\}^{\mathrm{T}}$ (FF01z) during the passage of a test train at a speed of 47.6 km/h.

Firstly, the response on the rail and the tunnel invert is considered. Fig. 8 shows the predicted and measured vertical velocity on the rail (A1) during the passage of the test train at a speed of 47.6 km/h. The contribution of each axle can clearly be distinguished (Fig. 8a), resulting in a quasi-discrete spectrum at low frequencies governed by the bogie and axle distances and the train speed (Fig. 8c). A peak corresponding to the axle passage frequency of $f_a = v/L_a = 6.92$ Hz ($L_a = 1.91$ m) is observed in the predicted as well as the measured spectra (Fig. 8c). The good agreement between the predicted quasi-static response at low frequencies below 8 Hz with the measurements indicates that the static stiffness of the track has been correctly modelled, which was unclear from the rail receptance measurement (Fig. 2). From the one-third octave band RMS spectra, it can be seen that the correspondence between predicted and experimental results around the wheel–track resonance frequency is reasonably good (Fig. 8d), which illustrates that the dynamic forces due to wheel and rail unevenness are properly estimated.

Fig. 9 shows the response at the tunnel invert. The quasi-static response has diminished on the tunnel invert. The dominant frequency content is situated in the frequency range above 30 Hz, where mainly the dynamic forces due rail/wheel unevenness and the rail joints are contributing. The vibration levels are maximum on the rail and decrease on the tunnel invert. The response at low frequencies between 5 and 12 Hz is underestimated by the numerical model. This could be due to the underestimation of the dynamic forces at these low frequencies. The influence of the train suspensions is also significant at low frequencies, which has been disregarded in the model. On the rail, however, the effect of the train suspensions is not that important as the quasi-static forces dominate the dynamic forces in the low frequency range.

Vibration measurements have also been performed in Regent's Park above the Bakerloo line tunnels. The vibration measurements have been performed on the surface as well as at a depth of 15 m, where tri-axial accelerometers have been installed in a seismic cone [31]. In this paper, the computed vertical response is compared to the measurements on the surface at $\{5.5\,\text{m}, 0\,\text{m}, 0\,\text{m}\}^{\text{T}}$ (FF01z) and $\{23.3\,\text{m}, 0\,\text{m}, 0\,\text{m}\}^{\text{T}}$ (FF02z) and at depth $\{23.3\,\text{m}, 0\,\text{m}, -15\,\text{m}\}^{\text{T}}$ (FF03z) (Fig. 10).

Figs. 11,12 and 13 compare the experimental and computed vertical free field vibration at points FF01z, FF02z and FF03z during the passage of a test train at a speed of 47.6 km/h. Both the experimental and

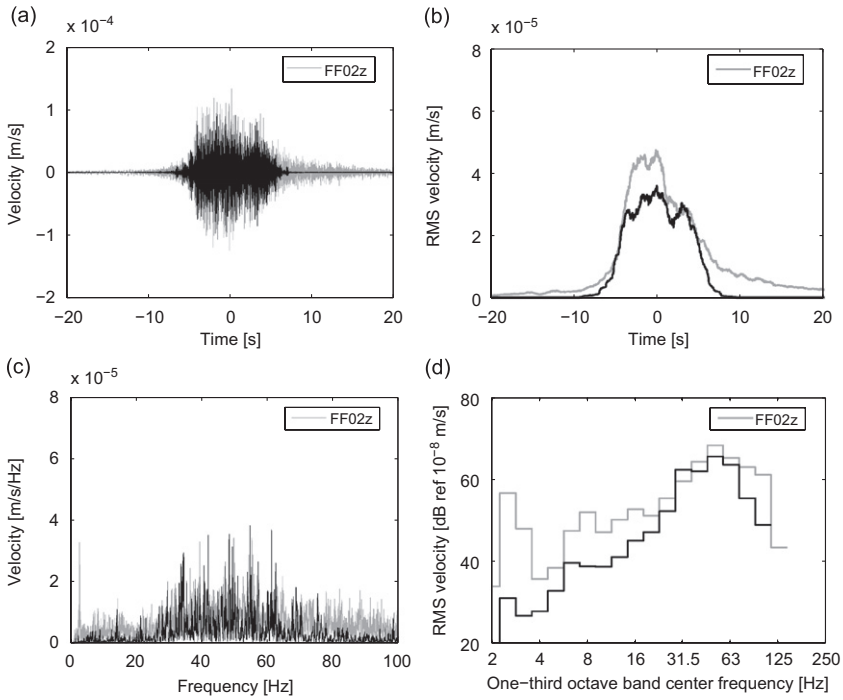

Fig. 12. Experimental (gray line) and computed (black line) (a) time history, (b) running RMS, (c) frequency content and (d) one-third octave band RMS spectra of the vertical velocity at $\{23.3\,\text{m}, 0\,\text{m}, 0\,\text{m}\}^{\text{T}}$ (FF02z) during the passage of a test train at a speed of 47.6 km/h.

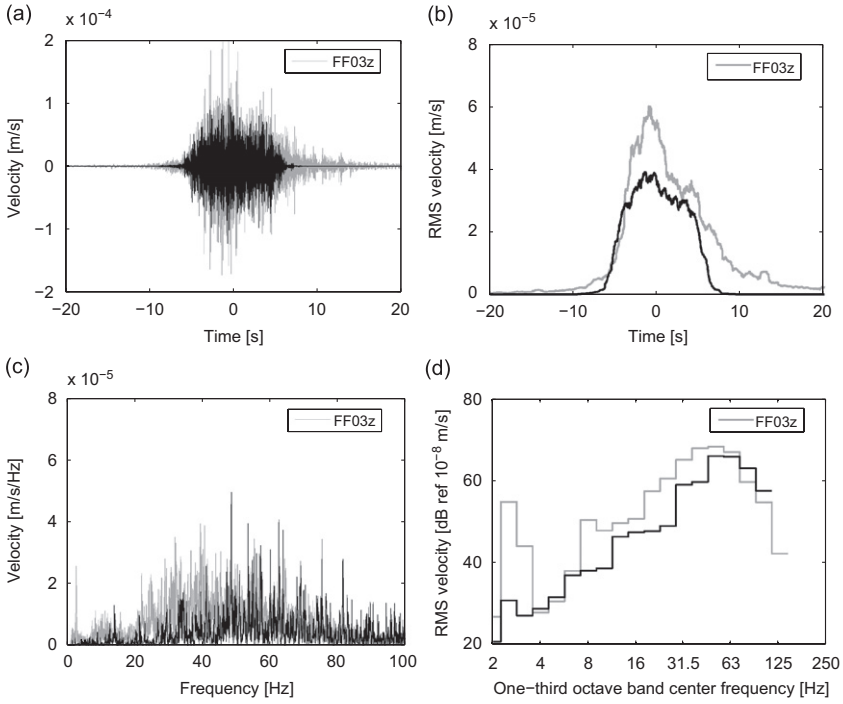

Fig. 13. Experimental (gray line) and computed (black line) (a) time history, (b) running RMS, (c) frequency content and (d) one-third octave band RMS spectra of the vertical velocity at $\{23.3\,\mathrm{m}, 0\,\mathrm{m}, -15\,\mathrm{m}\}^{\mathrm{T}}$ (FF03z) during the passage of a test train at a speeds 47.6 km/h.

numerical results show that the dominant frequency content is around the wheel–track resonance frequency of about 50 Hz. The bogie passages are not clearly visible in the time history of the response in the free field as the tunnel is situated at a considerable depth. The quasi-static contribution at low frequencies is not important in the free field and only the dynamic forces prevail. However, the dynamic forces at low frequencies have not been predicted well and thus the correspondence at low frequencies is not good. A relatively good agreement between the experimental and numerical results is observed for the response at points FF02z and FF03z at frequencies above 12 Hz. It can be observed that the vertical response at the surface (FF02z) has approximately the same magnitude as the vertical component at depth at the same location (FF03z). The response on the free surface at a lateral distance of 5.5 m from the tunnel (FF01z) is underestimated by the numerical model around the wheel–track resonance frequency between 30 and 80 Hz. Furthermore, the predicted response at FF01z is lower than the response at point FF02z, particularly in the frequency range between 30 and 80 Hz. This can be observed from the predicted transfer functions as well (Fig. 4). The amplification of the measured free field vibration at FF01z could probably be due to local site effects or inhomogeneities in the top layer. The agreement between the measurements and predictions is better for a point at depth (FF03z), which is located in the London clay. It may be noted that the background vibration levels have not been taken into consideration. This would partly account for the difference between the predicted and experimental results.

It is expected that higher frequency components attenuate with increasing distance from the tunnel due to material damping in the soil. This can be clearly observed in the predicted results but not in the measurements. This could be due to the inaccurate estimation of the material damping ratio in the soil.

4. Validation at other train speeds

In the following, 19 out of 35 passages of the test train in the Bakerloo line tunnel are considered. The train speed was varied between 20 and 50 km/h for the passages in the north-bound direction. The intention was to perform the experiments at varying speed for north-bound passages only. Eleven passages in the north-bound

direction at speeds 23.86, 24.19, 24.74, 32.53, 32.96, 37.36, 38.88, 44.34, 45.33, 46.40 and 47.60 km/h are considered in this paper. After each train passage in the north-bound direction, the test train returned to Regent's Park station at a constant speed of about 20 km/h. The measurements have been performed for these train passages as well and this has provided supplementary data. Eight passages in the south-bound direction at speeds 21.36, 21.78, 22.18, 23.41, 23.49, 23.50, 23.65 and 23.84 km/h are also considered. All events (north and south-bound passages) can be classified into four groups corresponding to speeds between: (1) 20–25 km/h (11 events), (2) 30–35 km/h (2 events), (3) 36–40 km/h (2 events) and (4) 44–48 km/h (4 events). The predictions have been made for one train speed from each set, i.e. for 23.86, 32.96, 38.88 and 47.6 km/h. The computations have been performed for a particular train speed, as the excitation force is estimated directly from the axle box vibrations using Eq. (5). If predictions have to be made for another train speed that is not considered in the experiments, the excitation force can be determined from Eq. (4) by approximating the unevenness with the measured axle box displacements as discussed in Section 2.4.

In the following, the running RMS and the one-third octave band RMS spectra of the measured and predicted vertical vibration velocity are compared. It should be remarked that set 1 consists of more events as additional experimental results for the train passages in the south-bound direction are available. Thus, a statistical analysis is performed on this data set by computing the mean value m and the standard deviation σ. Apart from the mean value m, the values $m \pm 1\sigma$ are displayed, which bounds a 68.3% confidence interval if it is assumed that the experimental data follow a Gaussian distribution. Since for other sets the number of events is limited, experimental results for all available train speeds are shown in the comparison.

Since the train speeds considered are relatively low, the variation in the response with train speed can directly be linked to the estimated axle loads. Fig. 14 shows the running RMS of the axle loads as a function of distance along the track and the one-third octave band RMS spectra of the axle loads. The one-third octave band RMS spectra of the axle loads are computed for a period of time corresponding to the passage of a train over the distance L_r between the first and the last axle of the train. The variation in the axle loads with train speed can be observed. For the three lower train speeds the peaks in the running RMS appear at the same location along the track, which are due to rail joints or other defects present on the track. It is crucial to identify the exact position of the train on the track for different speeds to compare the response on the rail and the tunnel invert. This is due to the fact that this response significantly varies along the track and can be attributed to the local influence of the rail joints. However, the response in the free field is not so sensitive to the exact position of the train along the track for different train speeds and is mainly determined by the average input power. For the train speed of 47.6 km/h, the axle load increases significantly and gives rise to higher levels of vibrations. This could be due to the high impact forces and possible wheel–rail separation at a higher speed [48], which has not been accounted for in the model. The maximum in the frequency domain occurs around the wheel–track resonance frequency between 50 and 100 Hz for all train speeds. Since the

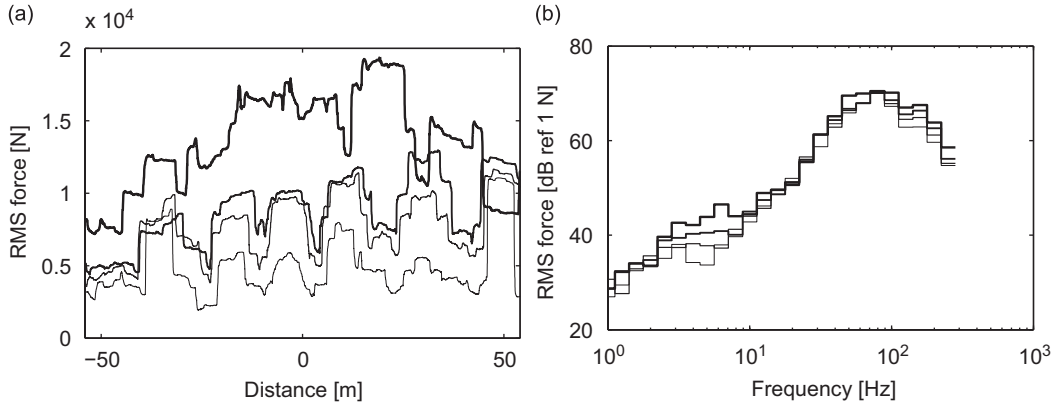

Fig. 14. (a) Running RMS and (b) one-third octave band RMS spectra of the estimated contact force at the front axle of the train for different train speeds (—— 47.6 km/h, —— 38.8 km/h, —— 32.96 km/h, —— 23.86 km/h; decreasing line thickness).

frequency range of interest is between 1 and 100 Hz, a low-pass filter with a cut-off frequency of 200 Hz is applied to the axle box vibrations in order to determine the axle loads.

Figs. 15 and 16 show the running RMS and the one-third octave band RMS spectra of the predicted velocity on the rail and the tunnel invert for the passages of the Bakerloo line tunnel at a speed of 23.86, 32.96, 38.8 and 47.6 km/h. For the events corresponding to set 1, the mean value m of the experimental RMS velocity and the $m \pm 1\sigma$ intervals are displayed (Figs. 15a and 16a). For sets 2–4, experimental results for all speeds are superimposed on the graphs. The predicted response is in good agreement with the measured response on the rail and tunnel invert for all four speeds considered. It can be observed that the length of the time window in the predictions as well as in the measurements is inversely proportional to the speed of the train. For the three lower speeds, the troughs in the running RMS velocity can be attributed to the passages of the bogies of the train. For the higher speed of 47.6 km/h, this pattern is not apparent as a consequence of higher impact forces on the rail. The RMS spectra at frequencies below 2 Hz should not be considered as a high-pass filter with a frequency of 2 Hz has been used in the processing of the data. The response on the rail and the tunnel invert is underestimated at lower frequencies between 5 and 20 Hz, which is due to underestimation of the dynamic forces at low frequencies. These differences are more pronounced at the tunnel invert for the three lower speeds. The dominant frequency content is above 30 Hz, where the correspondence between the predictions and measurements is reasonably good. The prediction accuracy on the rail and the tunnel invert for the considered train speeds is within 5 dB at frequencies above 20 Hz.

Figs. 17, 18 and 19 compare the running RMS and one-third octave band RMS spectra of the predicted and the measured velocity in the free field at $\{5.5\,\mathrm{m}, 0\,\mathrm{m}, 0\,\mathrm{m}\}^{\mathrm{T}}$ (FF01z), $\{23.3\,\mathrm{m}, 0\,\mathrm{m}, 0\,\mathrm{m}\}^{\mathrm{T}}$ (FF02z) and $\{23.3\,\mathrm{m}, 0\,\mathrm{m}, -15.0\,\mathrm{m}\}^{\mathrm{T}}$ (FF03z). The mean value m and $m \pm \sigma$ bounds of the experimental RMS velocity are shown for set 1, while all measurement results are displayed for other sets. The differences between the predictions and measurements in the free field at FF01z are considerable for all train speeds, which can be attributed to the uncertainty in the soil parameters. The correspondence between the computations and measurements is better at points FF02z and FF03z in the free field. The experimental running RMS values extend for a longer period than the predicted running RMS. This reflects the contribution of some noise in the data. Furthermore, the unevenness outside a stretch of length $L_r = 216\,\mathrm{m}$ has not been considered in the analysis, which may have some influence on the starting and end part of the predicted response. The stationary part of the response, however, is mainly influenced by the unevenness in the considered zone.

The contribution of the quasi-static forces is negligible in the free field. The dominant frequency content is between 30 and 100 Hz, where lies the wheel–track resonance frequency. The dynamic forces due to rail-wheel unevenness, rail joints and the parametric excitation are contributing to the response in the free field. The discrepancy between the computations and the experiments is larger in the free field than in the tunnel. However, the correspondence around the wheel–track resonance frequency of about 52 Hz is reasonably good and the difference between the computations and experiments is less than 10 dB for points FF02z and FF03z in the free field. The predicted as well as measured vibration levels in the free field are much lower than $2 \times 10^{-4}\,\mathrm{m/s}$, the limit for human perception.

From these results, it can be seen that the general trend in the variation of the response with train speeds is similar for measurements as well as predictions. To quantify the speed dependance, the maximum of the RMS velocity is plotted as a function of train speed. The reason for considering the maximum RMS velocity instead of the peak particle velocity is that people respond to the average vibration amplitude during 1 s rather than the peak value [49].

As mentioned before, the dependence of the response is directly proportional to the estimated wheel/track interaction force as the considered train speeds are very low. Fig. 20 shows the maximum RMS levels of the contact force at different speeds. The linear regression on the data shows a moderate increase in the force with train speeds. The increase in the force with speed can be associated to the unevenness and rail joints present on the track. Theoretically, unevenness is modelled as a random process characterized by a single sided power spectral density [50,51]. In the present case, it is difficult to relate the variation in the dynamic force with one of these PSD curves, as the dynamic forces are induced by the unevenness as well as the rail joints.

Fig. 21 shows the maximum RMS velocity of the response on the rail (A1) and the tunnel invert (A6). It can be seen that the trend in the variation of the force and the response is very similar. Superimposed on the same

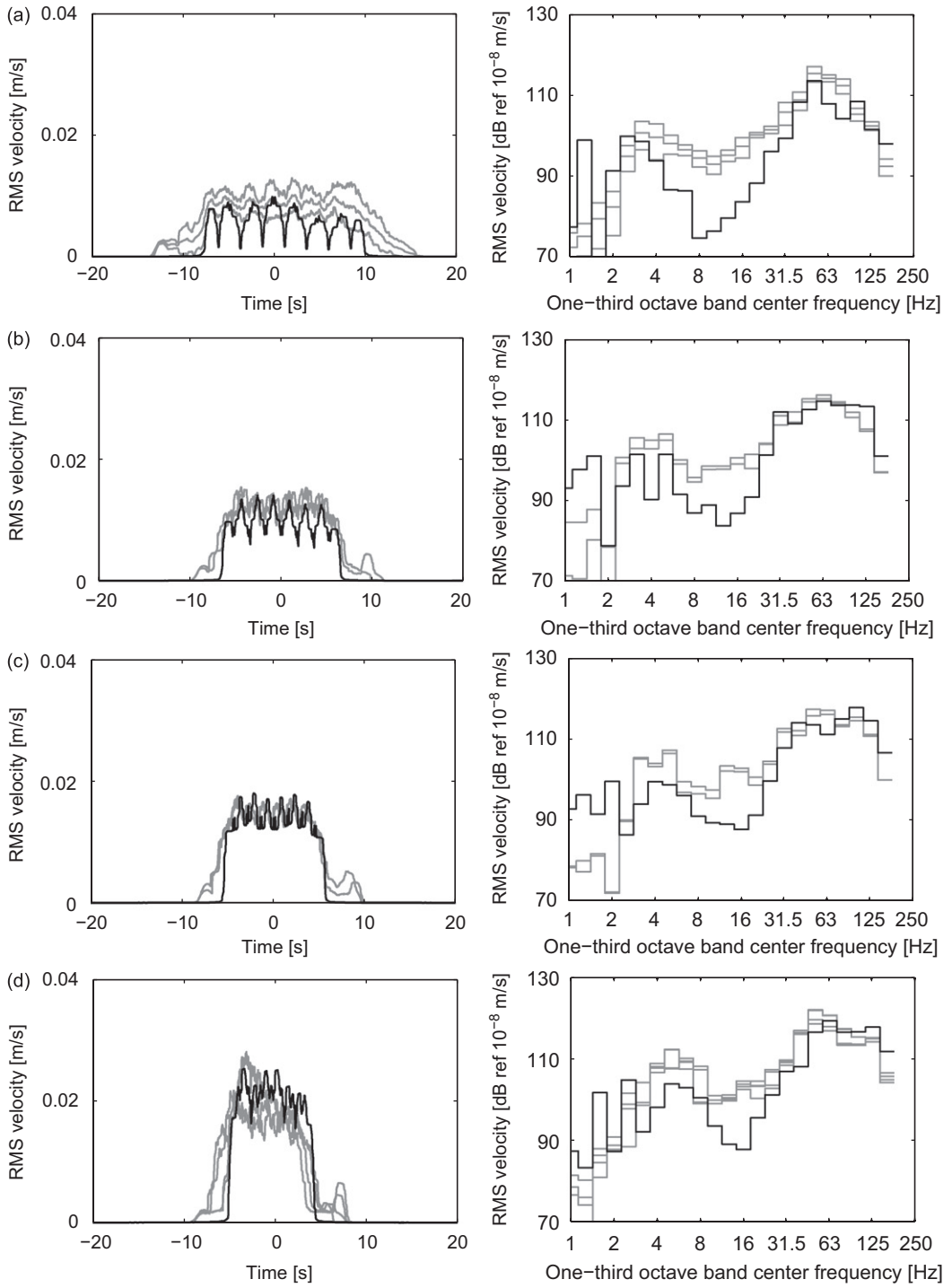

Fig. 15. Computed (solid black line) running RMS and one-third octave band RMS spectra of the vertical velocity on the rail (A1) for the train passages at a speed of (a) 23.86 km/h, (b) 32.96 km/h, (c) 38.8 km/h and (d) 47.6 km/h. Superimposed on (a) are the values m and $m \pm 1\sigma$ of the experimental data (gray lines) belonging to set 1. Superimposed on (b), (c) and (d) are the experimental results (gray lines) for sets 2, 3 and 4, respectively.

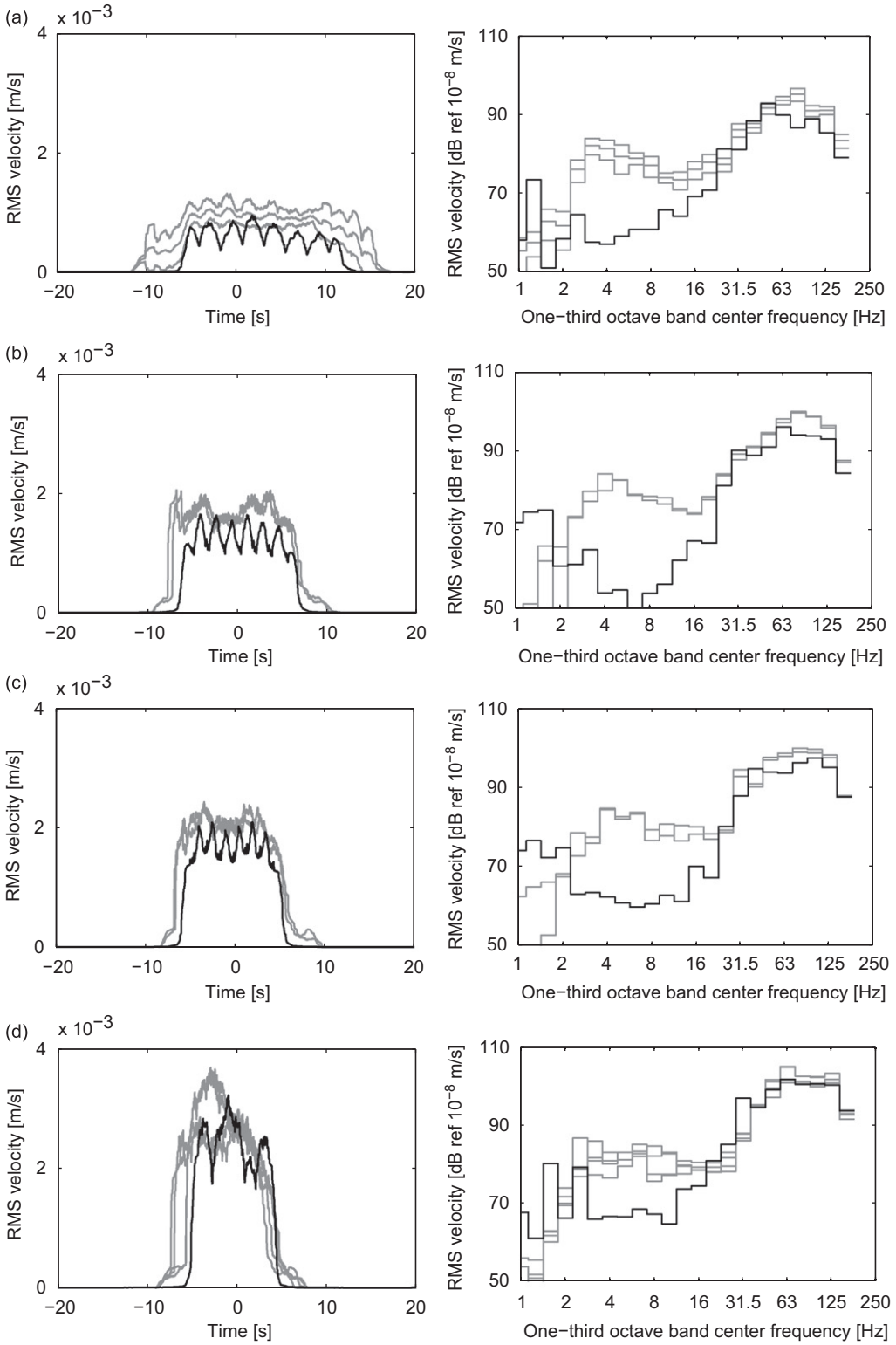

Fig. 16. Computed (solid black line) running RMS and one-third octave band RMS spectra of the vertical velocity on the tunnel invert (A6) for the train passages at a speed of (a) 23.86 km/h, (b) 32.96 km/h, (c) 38.8 km/h and (d) 47.6 km/h. Superimposed on (a) are the values m and $m \pm 1\sigma$ of the experimental data (gray lines) belonging to set 1. Superimposed on (b), (c) and (d) are the experimental results (gray lines) for sets 2, 3 and 4, respectively.

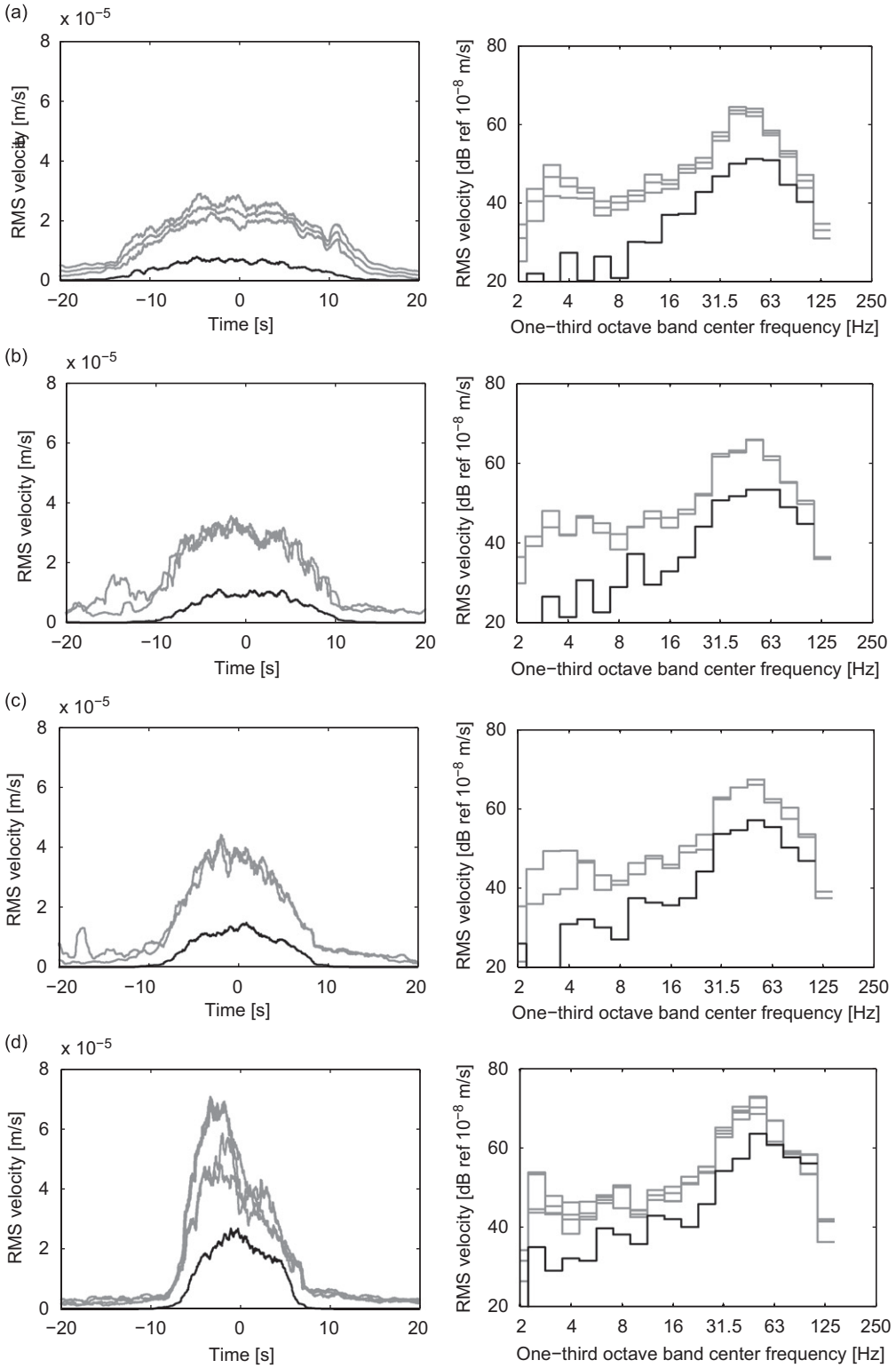

Fig. 17. Computed (solid black line) running RMS and one-third octave band RMS spectra vertical velocity in the free field at $\{5.5\,\mathrm{m}, 0\,\mathrm{m}, 0\,\mathrm{m}\}^{\mathrm{T}}$ (FF01z) for the train passages at a speed of (a) 23.86 km/h, (b) 32.96 km/h, (c) 38.8 km/h and (d) 47.6 km/h. Superimposed on (a) are the values m and $m \pm 1\sigma$ of the experimental data (gray lines) belonging to set 1. Superimposed on (b), (c) and (d) are the experimental results (gray lines) for sets 2, 3 and 4, respectively.

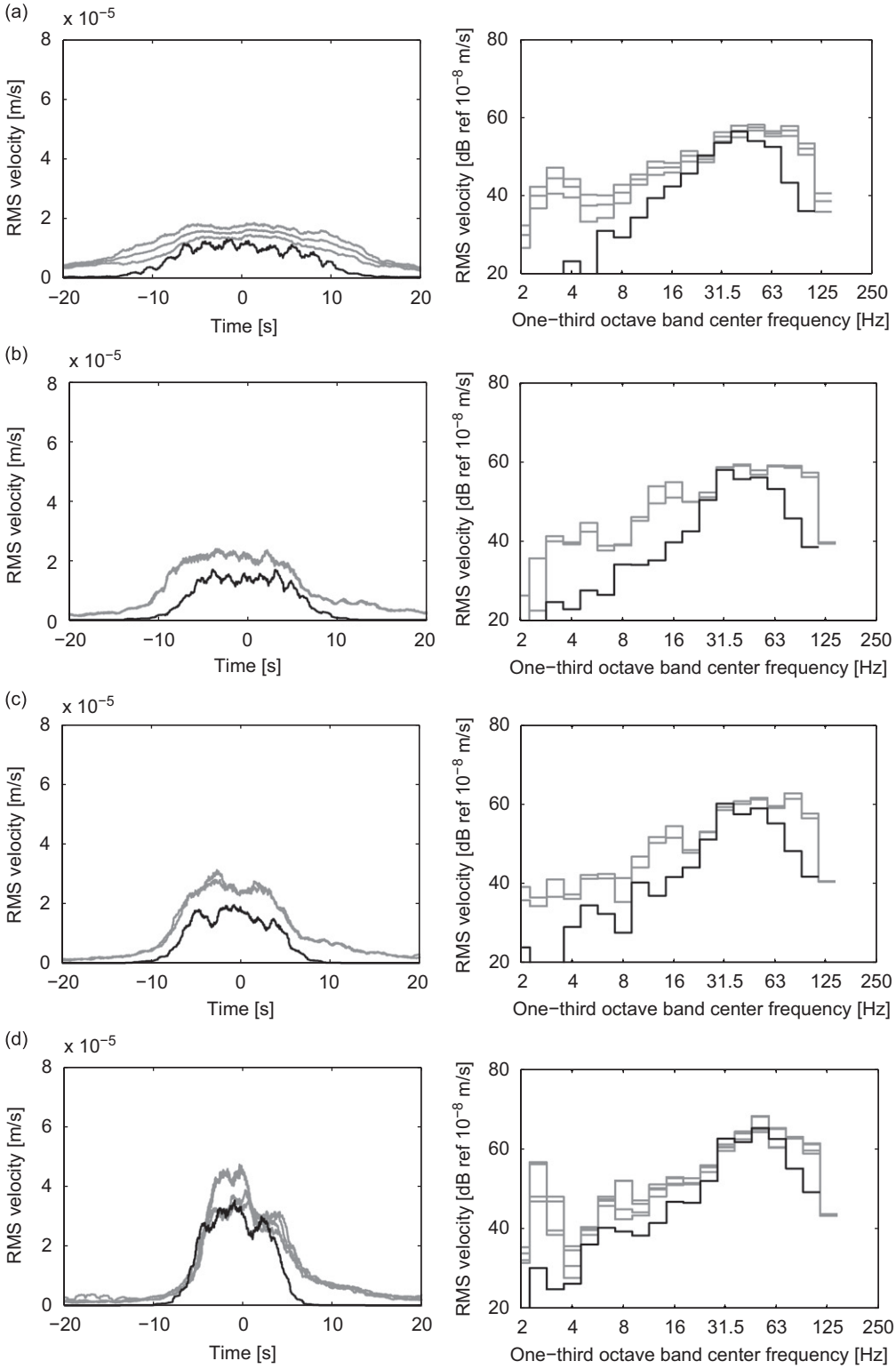

Fig. 18. Computed (solid black line) running RMS and one-third octave band RMS spectra vertical velocity in the free field at $\{23.3\,\mathrm{m}, 0\,\mathrm{m}, 0\,\mathrm{m}\}^{\mathrm{T}}$ (FF02z) for the train passages at a speed of (a) 23.86 km/h, (b) 32.96 km/h, (c) 38.8 km/h and (d) 47.6 km/h. Superimposed on (a) are the values m and $m \pm 1\sigma$ of the experimental data (gray lines) belonging to set 1. Superimposed on (b), (c) and (d) are the experimental results (gray lines) for sets 2, 3 and 4, respectively.

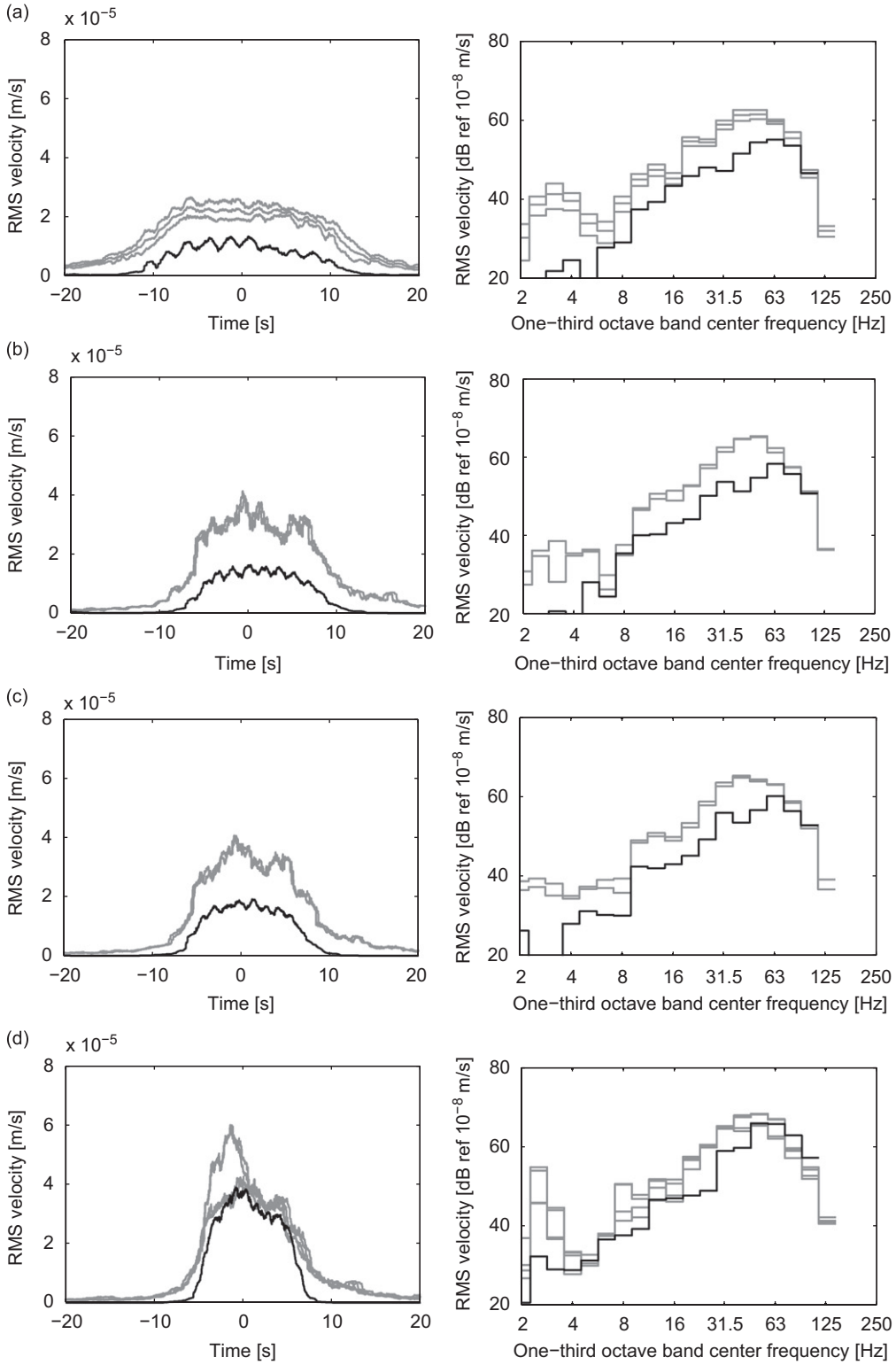

Fig. 19. Computed (solid black line) running RMS and one-third octave band RMS spectra vertical velocity in the free field at $\{23.3\,\mathrm{m}, 0\,\mathrm{m}, -15\,\mathrm{m}\}^{\mathrm{T}}$ (FF03z) for the train passages at a speed of (a) 23.86 km/h, (b) 32.96 km/h, (c) 38.8 km/h and (d) 47.6 km/h. Superimposed on (a) are the values m and $m \pm 1\sigma$ of the experimental data (gray lines) belonging to set 1. Superimposed on (b), (c) and (d) are the experimental results (gray lines) for sets 2, 3 and 4, respectively.

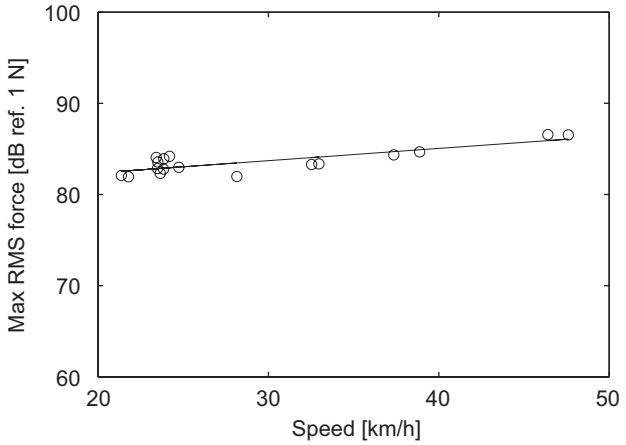

Fig. 20. Maximum RMS levels of the force at different train speeds.

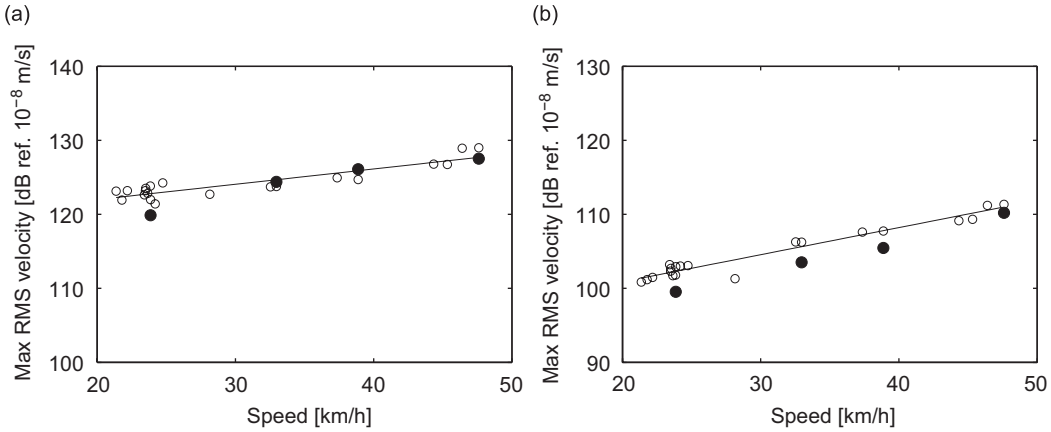

Fig. 21. Experimental (empty circles) and computed (filled circles) maximum RMS velocity on (a) the rail (A1) and (b) the tunnel invert (A6).

graphs are the predictions at train speeds 23.86, 32.96, 38.88 and 47.60 km/h. The difference between the experimental and predicted results is less than 5 dB for the points in the tunnel.

Fig. 22 shows the maximum RMS velocity of the response at 10 points in the free field. Points FF01z, FF02z, FF03z, FF04z and FF05z are located on line 1 perpendicular to the tunnel, while points FF06z, FF07z, FF08z, FF09z and FF10z are on line 2 (Fig. 10). The increase in the predicted response is approximately the same as shown by a linear fit on the measurement data, i.e. doubling the train speed increases the vibration levels by 4–6 dB. This trend is quite generic, as it is also observed on other sites and stated in a report by FRA [49]. At points FF01z and FF06z, the difference between the maximum RMS velocity for the experiments and predictions is very large, which can be attributed to uncertainty in the soil parameters and variations due to local site conditions. The difference is less than 10 dB at the observation points FF02z, FF03z, FF07z and FF08z. At larger distances from the tunnel (FF04z, FF05z, FF09z, FF10z), the agreement between the experimental and predicted results is poor. It can be observed that the attenuation in the response along lines 1 and 2 is largely overestimated by the numerical model. This can be due to a inaccurate estimation of the material damping ratio in the soil, which is an important parameter for reasonable predictions at large distances from the source. To elucidate the importance of the material damping ratio, the experimental results are also compared to the maximum RMS velocity calculated by halving the material damping ratio. The correspondence between the predicted and experimental results improves at large distances. As mentioned earlier, the material damping ratio has been determined by laboratory testing on

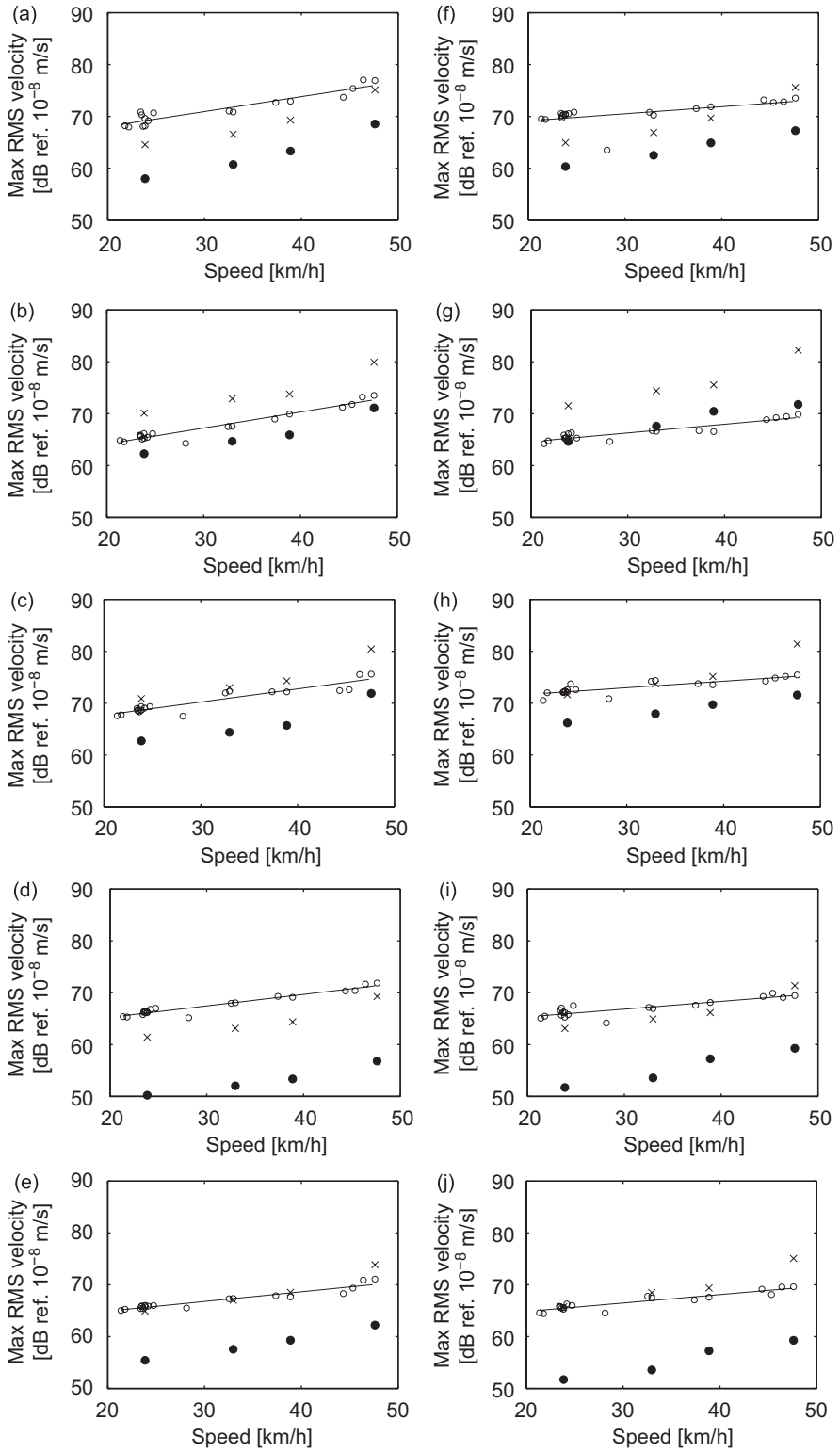

Fig. 22. Experimental (empty circles) and computed (filled circles) maximum RMS velocity in the free field at (a) FF01z, (b) FF02z, (c) FF03z, (d) FF04z, (e) FF05z, (f) FF06z, (g) FF07z, (h) FF08z, (i) FF09z and (j) FF10z for different train speeds. Superimposed on the graphs is the maximum RMS velocity computed by halving the material damping ratio of the soil (crosses).

undisturbed samples from the site. However, these values may not give a good representation of the material damping ratio in the entire soil domain. Several methods [52,53] have been developed to determine the material damping ratio from in situ tests. These techniques must be applied to estimate a suitable value of the material damping ratio that can be used for prediction of ground-borne vibrations using the numerical tools.

The moderate dependence on the speed is observed for all observation points in the tunnel and in the free field.

5. Conclusions

In this paper, the experimental validation of a numerical model for the prediction of subway induced vibrations has been presented. An elaborate measurement campaign has been conducted at a site in Regent's Park situated above the Bakerloo line tunnels of London Underground in order to validate the numerical model.

The coupled periodic finite element–boundary element model fully accounts for the dynamic interaction between the train, the track, the tunnel and the soil. The response to moving loads (trains) is computed by first estimating the excitation forces and then solving the track–tunnel–soil interaction problem to compute the vibrations in the tunnel and the free field. The interaction force determined from the axle box vibrations accounts for various excitation mechanisms such as unevenness excitation, excitation due to rail joints and parametric excitation. The vibrations in the tunnel as well as in the free field have been predicted and validated for the passage of a test train in the Bakerloo line. The correspondence between the predicted and experimental results is reasonably good, given the large number of modelling uncertainties. The following conclusions can be drawn from the present analysis:

(1) The agreement between the predictions and measurements is better in the tunnel than in the free field. The discrepancy in the free field can be attributed to the uncertainty in the dynamic soil properties. The top layer has been observed inhomogeneous from the in situ tests (SCPT and CPT) and this may have resulted in a large difference between the predictions and measurements at points FF01z and FF06z in the free field, which are located on the free surface close to the tunnel. At points further away from the tunnel (FF02z, FF03z, FF07z and FF08z) the prediction accuracy is within 10 dB.
At larger distances from the tunnel (FF04z, FF05z, FF09z and FF10z) the predicted response is severely underestimated, which can be attributed to a relatively high value of the material damping ratio used in the computations. The material damping ratio is an important parameter for accurate predictions in the free field, particularly at large distances from the source. This is demonstrated by considering a lower value of the material damping ratio. It has been observed that the maximum RMS velocity increases by about 10 dB, when the material damping ratio is halved. Therefore, it is desirable to correctly determine the material damping ratio from in situ tests, rather than from laboratory testing of soil samples. It should also be remembered that, for accurate predictions in the free field, it is important to precisely know the properties of the soil around the tunnel, which was not possible in the present case as the tunnel is situated at a considerable depth.
(2) The differences between the predictions and measurements at frequencies less than 15 Hz, can be attributed to the underestimation of the dynamic forces. This could be partly because the train suspensions have been disregarded, and partly because some of the excitation mechanisms are not properly represented in the axle box vibrations. For example, distinct peaks at the sleeper passage frequency between 5 and 15 Hz for different speeds between 20 and 50 km/h are not observed in the measurements as well as the predictions.
(3) The general trend in the variation of the response with train speed is similar for the predictions as well as the measurements. An increase of 4–6 dB in the maximum RMS velocity is observed by doubling the train speed. This dependence is related to the variation in the wheel/track interaction forces arising due to the rail and wheel unevenness and the rail joints.

This paper demonstrates that the coupled periodic finite element–boundary element model can be used to make realistic predictions provided a careful consideration is given to the modelling of the vehicle, track,

tunnel and the soil. As a large amount of uncertainty is still involved in the problem, it is difficult to achieve a prediction accuracy of better than 10 dB.

Acknowledgments

The results presented in this paper have been obtained within the frame of the SBO project IWT 03175 "Structural damage due to dynamic excitation: a multi-disciplinary approach", funded by IWT Vlaanderen. This financial support is gratefully acknowledged.

The third author is a Postdoctoral Fellow of the Research Foundation—Flanders (FWO). The support of the FWO is gratefully acknowledged.

References

[1] Y.B. Yang, L.C. Hsu, A review of researches on ground-borne vibrations due to moving trains via underground tunnels, *Advances in Structural Engineering* 9 (3) (2006) 377–392.
[2] L.G. Kurzweil, Ground-borne noise and vibration from underground rail systems, *Journal of Sound and Vibration* 66 (3) (1979) 363–370.
[3] J. Melke, Noise and vibration from underground railway lines: proposals for a prediction procedure, *Journal of Sound and Vibration* 120 (1988) 391–406.
[4] R.A. Hood, R.J. Greer, M. Breslin, P.R. Williams, The calculation and assessment of ground-borne noise and perceptible vibration from trains in tunnels, *Journal of Sound and Vibration* 193 (1996) 215–225.
[5] A. Trochides, Ground-borne vibrations in buildings near subways, *Applied Acoustics* 32 (1991) 289–296.
[6] K.H. Chua, T. Balendra, K.W. Lo, Groundborne vibrations due to trains in tunnels, *Earthquake Engineering and Structural Dynamics* 21 (5) (1992) 445–460.
[7] K.H. Chua, K.W. Lo, T. Balendra, Building response due to subway train traffic, *Journal of Geotechnical Engineering, Proceedings of the ASCE* 121 (11) (1995) 747–754.
[8] W. Rücker, S. Said, *Erschütterungsübertragung zwischen U-Bahn-Tunneln und dicht benachbarten Gebäuden*, Forschungsbericht 199, Bundesanstalt für Materialforschung und -prüfung, Berlin, 1994.
[9] C.J.C. Jones, D.J. Thompson, M. Petyt, A model for ground vibration from railway tunnels, *Transport* 153 (2) (2002) 121–129.
[10] M. Mohammadi, D.L. Karabalis, Dynamic 3-d soil-railway track interaction by BEM-FEM, *Earthquake Engineering and Structural Dynamics* 24 (1995) 1177–1193.
[11] O. von Estorff, M. Firuziaan, K. Friedrich, G. Pflanz, G. Schmid, A three-dimensional FEM/BEM model for the investigation of railway tracks, in: N. Chouw, G. Schmid (Eds.), *Proceedings of the International Workshop Wave 2000, Wave Propagation, Moving Load, Vibration Reduction*, Ruhr University, Germany, A.A. Balkema, Rotterdam, December 2000, pp. 157–172.
[12] K. Abe, D. Satou, T. Suzuki, M. Furuta, Three-dimensional analysis of subway track vibrations due to running wheels, in: N. Chouw, G. Schmid (Eds.), *Proceedings of the International Workshop Wave 2000, Wave Propagation, Moving Load, Vibration Reduction*, Ruhr University, Germany, A.A. Balkema, Rotterdam, December 2000, pp. 149–156.
[13] A.A. Stamos, D.E. Beskos, Dynamic analysis of large 3-D underground structures by the BEM, *Earthquake Engineering and Structural Dynamics* (1995) 1–18.
[14] A.A. Stamos, D.E. Beskos, 3-D seismic response analysis of long lined tunnels in half-space, *Soil Dynamics and Earthquake Engineering* 15 (1996) 111–118.
[15] X. Sheng, C.J.C. Jones, D.J. Thompson, Prediction of ground vibration from trains using the wavenumber finite and boundary element methods, *Journal of Sound and Vibration* 293 (2006) 575–586.
[16] L. Andersen, C.J.C. Jones, Coupled boundary and finite element analysis of vibration from railway tunnels—a comparison of two- and three-dimensional models, *Journal of Sound and Vibration* 293 (2006) 611–625.
[17] Y.B. Yang, H.H. Hung, A 2.5D finite/infinite element approach for modeling visco-elastic bodies subjected to moving loads, *International Journal for Numerical Methods in Engineering* 51 (2001) 1317–1336.
[18] Y.B. Yang, H.H. Hung, Train-induced wave propagation in layered soil using finite/infinite element simulation, *Soil Dynamics and Earthquake Engineering* 23 (4) (2003) 263–278.
[19] G. Lombaert, G. Degrande, Experimental validation of a numerical prediction model for free field traffic induced vibrations by in situ experiments, *Soil Dynamics and Earthquake Engineering* 21 (6) (2001) 485–497.
[20] G. Lombaert, G. Degrande, J. Kogut, S. François, The experimental validation of a numerical model for the prediction of railway induced vibrations, *Journal of Sound and Vibration* 297 (3–5) (2006) 512–535.
[21] ⟨http://www.convurt.com⟩, 2003.
[22] M.F.M. Hussein, H.E.M. Hunt, A numerical model for calculating vibration from a railway tunnel embedded in a full-space, *Journal of Sound and Vibration* 305 (5) (2007) 401–431.
[23] M.F.M. Hussein, L. Rikse, S. Gupta, H.E.M. Hunt, G. Degrande, J.P. Talbot, S. François, M. Schevenels, Using the PiP model for fast calculation of vibration from a railway tunnel in a multi-layered half-space, *9th International Workshop on Railway Noise*, Munich, Germany, September 2007.

[24] J.A. Forrest, H.E.M. Hunt, A three-dimensional tunnel model for calculation of train-induced ground vibration, *Journal of Sound and Vibration* 294 (2006) 678–705.
[25] D. Clouteau, M. Arnst, T.M. Al-Hussaini, G. Degrande, Freefield vibrations due to dynamic loading on a tunnel embedded in a stratified medium, *Journal of Sound and Vibration* 283 (1–2) (2005) 173–199.
[26] G. Degrande, M. Schevenels, P. Chatterjee, W. Van de Velde, P. Hölscher, V. Hopman, A. Wang, N. Dadkah, Vibrations due to a test train at variable speeds in a deep bored tunnel embedded in London clay, *Journal of Sound and Vibration* 293 (3–5) (2006) 626–644.
[27] S. Gupta, M.F.M. Hussein, G. Degrande, H.E.M. Hunt, D. Clouteau, A comparison of two numerical models for the prediction of vibrations from underground railway traffic, *Soil Dynamics and Earthquake Engineering* 27 (7) (2007) 608–624.
[28] H. Chebli, O. Ramzi, D. Clouteau, Response of periodic structures due to moving loads, *Comptes Rendus Mécanique* 334 (2006) 347–352.
[29] S. Gupta, W. Liu, G. Degrande, G. Lombaert, W. Liu, Prediction of vibrations induced by underground railway traffic in Beijing, *Journal of Sound and Vibration* 310 (2008) 608–630.
[30] A. Wang, Track measurements on London Underground Bakerloo Line, Report 16487-2, Pandrol, May 2003, CONVURT EC-Growth Project G3RD-CT-2000-00381.
[31] P. Hölscher, V. Hopman, Test site Regent's Park London. Soil description, Report 381540-104, Version 2, GeoDelft, December 2003, CONVURT EC-Growth Project G3RD-CT-2000-00381.
[32] G. Degrande, D. Clouteau, R. Othman, M. Arnst, H. Chebli, R. Klein, P. Chatterjee, B. Janssens, A numerical model for ground-borne vibrations from underground railway traffic based on a periodic finite element—boundary element formulation, *Journal of Sound and Vibration* 293 (3–5) (2006) 645–666.
[33] X. Sheng, C.J.C. Jones, D.J. Thompson, A comparison of a theoretical model for quasi-statically and dynamically induced environmental vibration from trains with measurements, *Journal of Sound and Vibration* 267 (3) (2003) 621–635.
[34] H.E.M. Hunt, M.F.M. Hussein, Vibration from railways: Can we achieve better than $+/-10$ dB prediction accuracy? *Proceedings of the 14th International Congress on Sound and Vibration*, Cairns, Australia, July 2007.
[35] M. Schevenels, G. Lombaert, G. Degrande, S. François, A probabilistic assessment of resolution in the SASW test and its impact on the prediction of ground vibrations, *Geophysical Journal International* 172 (1) (2008) 262–275.
[36] S. Gupta, G. Degrande, H. Chebli, D. Clouteau, M.F.M. Hussein, H.E.M. Hunt, A coupled periodic FE–BE model for ground-borne vibrations from underground railways, in: C.A. Mota Soares (Ed.), *Proceedings of the 3rd European Conference on Computational Mechanics*, Lisbon, Portugal, June 2006.
[37] F.J. Rizzo, D.J. Shippy, An application of the correspondence principle of linear viscoelasticity theory, *SIAM Journal on Applied Mathematics* 21 (2) (1971) 321–330.
[38] M. Schevenels, The Impact of Uncertain Dynamic Soil Characteristics on the Prediction of Ground Vibrations, Ph.D. Thesis, Department of Civil Engineering, K.U. Leuven, 2007.
[39] H. Takemiya, X. Bian, Substructure simulation of inhomogeneous track and layered ground dynamic interaction under train passage, *Journal of Engineering Mechanics* 131 (2005) 699–711.
[40] X. Sheng, C.J.C. Jones, D.J. Thompson, Response of infinite periodic structures to moving or stationary harmonic loads, *Journal of Sound and Vibration* 282 (2005) 125–149.
[41] A.V. Vostroukhov, A.V. Metrikine, Periodically supported beam on a visco-elastic layer as a model for dynamic analysis of a high-speed railway track, *International Journal of Solids and Structures* 40 (2003) 5723–5752.
[42] D. Clouteau, M.L. Elhabre, D. Aubry, Periodic BEM and FEM–BEM coupling: application to seismic behaviour of very long structures, *Computational Mechanics* 25 (2000) 567–577.
[43] S. Gupta, G. Degrande, A comparison of prediction models for vibrations from underground railway traffic, Report BWM-2005-15, Department of Civil Engineering, K.U. Leuven, November 2005, SBO Project IWT 03175.
[44] R.J. Diehl, H. Holm, Roughness measurements—-Have the necessities changed?, *Journal of Sound and Vibration* 293 (2006) 777–783.
[45] International Organization for Standardization, ISO 3095:2005: railway applications—acoustics—measurement of noise emitted by railbound vehicles, 2005.
[46] International Organization for Standardization, ISO 2631-2:1999: mechanical vibration and shock—evaluation of human exposure to whole-body vibration—Part 2: Vibration in buildings (1 to 80 Hz), 1999.
[47] Deutsches Institut für Normung, DIN 45672 Teil 2: Schwingungsmessungen in der Umgebung von Schienenverkehrswegen: Auswerteverfahren, 1995.
[48] T.X. Wu, D.J. Thompson, On the impact noise generation due to a wheel passing over rail joints, *Journal of Sound and Vibration* 267 (2003) 485–496.
[49] Federal Railroad Administration, High-speed ground transportation noise and vibration impact assessment: HMMH Report No. 293630-4, 2005.
[50] A. Hamid, T.L. Yang, Analytical description of track-geometry variations, *Transportation Research Record* 838 (1981) 19–26.
[51] H. Braun, T. Hellenbroich, Messergebnisse von Strassenunebenheiten, *VDI Berichte* 877 (1991) 47–80.
[52] M. Schevenels, S.A. Badsar, G. Lombaert, G. Degrande, Robust ground vibration predictions based on SASW tests, *Proceedings of the Inaugural International Conference of the Engineering Mechanics Institute (EM08)*, Minneapolis, Minnesota, USA, May 2008.
[53] G.J. Rix, C.G. Lai, A.W. Spang Jr., In situ measurement of damping ratio using surface waves, *Journal of Geotechnical and Geoenvironmental Engineering, Proceedings of the ASCE* 126 (5) (2000) 472–480.